HHS Public Access

Author manuscript

Neurosurg Clin N Am. Author manuscript; available in PMC 2017 October 01.

Published in final edited form as:

Neurosurg Clin N Am. 2016 October ; 27(4): 409–439. doi:10.1016/j.nec.2016.05.011.

Imaging Evaluation of Acute Traumatic Brain Injury

Christopher A. Mutch, MD, PhD [PGY5 Radiology Resident],
Department of Radiology, UCSF, San Francisco, CA

Jason F. Talbott, MD, PhD [Assistant Professor], and
Department of Radiology, UCSF and SFGH, San Francisco, CA

Alisa Gean, MD [Professor Emeritus]
Department of Radiology; Adjunct Professor Emeritus of Neurology and Neurosurgery, UCSF and SFGH, San Francisco, CA

SYNOPSIS

Traumatic brain injury (TBI) is a major cause of morbidity and mortality worldwide. Imaging plays an important role in the evaluation, diagnosis, and triage of patients with TBI. Recent studies suggest that it will also help predict patient outcomes. TBI consists of multiple pathoanatomical entities. Here we review the current state of TBI imaging including its indications, benefits and limitations of the modalities, imaging protocols, and imaging findings for each these pathoanatomic entities. We also briefly survey advanced imaging techniques, which include a number of promising areas of TBI research.

Keywords

Traumatic Brain Injury; TBI; Imaging; MRI; CT

INTRODUCTION

In the United States, traumatic brain injury (TBI) is estimated to affect 1.7 million people annually, leading to approximately 52,000 deaths and 275,000 hospitalizations. TBI plays a role in approximately one third of all injury related deaths[1]. Patients who survive the initial event can have debilitating long-term sequelae. TBI actually consists of multiple

CORRESPONDING AUTHOR Jason F. Talbott, MD, PhD, jason.talbott@ucsf.edu, San Francisco General Hospital, 1001 Potrero Ave., San Francisco, CA 94110.

AUTHOR CONTACT INFORMATION
Christopher A. Mutch, MD, PhD, christopher.mutch@ucsf.edu, University of California, San Francisco, 505 Parnassus Ave., M391, San Francisco, CA 94143
Alisa Gean, MD, alisa.gean@ucsf.edu, San Francisco General Hospital, 1001 Potrero Ave., San Francisco, CA 94110

DISCLOSURE STATEMENT
JFT is member of a data monitoring committee for StemCells, Inc. Phase II clinical trial for stem cells in spinal cord injury.
CAM and ADG have nothing to disclose.

pathological entities broadly defined by an “alteration in brain function, or other evidence of brain pathology, caused by an external force[2].” Imaging plays a crucial role in evaluation and diagnosis of TBI, particularly relevant is its role for triage in the acute setting for determination of which patients require emergent neurosurgical intervention. Thus, the treating practitioner and radiologist must be familiar with the various imaging manifestations of TBI pathology and their impact on clinical presentation, management, and prognosis.

The damage incurred by TBI can be differentiated into primary and secondary mechanisms. Primary injury is typically defined as the direct mechanical damage caused by trauma. These injuries are usually apparent acutely and include fractures, intracranial hemorrhage, contusion and traumatic axonal injury. This type of injury is best detected with conventional CT and MR structural imaging techniques. Secondary injury mechanisms are varied, and relate to disruption of the blood brain barrier, production of reactive oxygen species and resultant oxidative stress, metabolic dysfunction, inflammation and excitotoxicity [3, 4]. These processes are mediated at the cellular level which is currently below the resolution of conventional imaging; however, they are believed to greatly contribute to the long term morbidity and disability associated with TBI. When severe, macroscopic manifestations of secondary injuries may become apparent as diffuse cerebral hyperemia, cytotoxic and/or vasogenic edema, and tissue ischemia,

Clinical examination remains the cornerstone of acute TBI assessment. There are numerous clinical classification systems for TBI based on symptomology and severity, the most entrenched of which is the Glasgow Coma Scale (GCS) [5] The GCS is a clinical assessment tool with scores ranging from 3 to 15 based upon three components of neurologic function: 1) eye opening to external stimuli, 2) motor response to stimuli, and 3) verbal response. TBI is commonly subdivided into mild (≥13), moderate (9-12) and severe grade (3-8) using the GCS (Table 1.) While the GCS score has been shown to correlate with outcomes, it has limitations. Different varieties of pathoanatomic lesions can result in low GCS scores at admission[6]. For example, initial low GCS scores may be seen with subdural hematomas (SDHs), epidural hematomas (EDHs), cortical contusions, intracerebral hematomas (ICHs), and traumatic axonal injury (TAI), though, these lesions may have very different clinical courses and long-term prognoses[6, 7]. Evaluation is also limited by sedation, paralysis, and pre-existing injuries. Despite these limitations, the GCS has relatively high inter-rater reliability and does an adequate job of quickly and accurately stratifying patients broadly based on clinical severity of injury. GCS subscores should always be reported to convey a more granular description of neurologic impairment instead of simply reporting the composite score, which is less meaningful in isolation.

In conjunction with neurologic exam and clinical history, pathoanatomic characterization of TBI lesions with imaging is critical for triage and prognostication. In order to standardize definitions and imaging protocols for TBI classification and to promote research, the Interagency Common Data Elements Project was established in 2008[8]. Throughout the following descriptions of TBI injury classification and imaging protocols, we attempt to adhere to the common data element pathoanatomic terminologies and recommendations[9, 10]. We will begin with a brief summary of modality-specific indications for TBI. Technical

considerations and neuroimaging protocols will also be examined. Characteristic findings associated with the most frequently encountered extra-axial and intra-axial pathoanatomic lesions will then be described. Finally, a brief review of advanced imaging techniques for TBI evaluation will be reviewed. Throughout, we aim to highlight how standardized imaging-based characterization of pathoanatomic lesions may complement clinical assessment for optimal triage and management of TBI patients.

ROUTINE CLINICAL IMAGING

Routine clinical imaging for suspected traumatic brain injury typically consists of noncontrast CT and MRI in select cases[11, 12]. Cases of known and suspected primary vascular abnormality may require the addition of noninvasive angiography (CT angiography or MR angiography) or catheter angiography for diagnosis, and in some cases, treatment. In the past, skull radiographs were performed as a first-line study to evaluate for calvarial fractures in children (Figure 1), though, this has fallen out of favor because significant intracranial pathology can occur in absence of skull fracture[13]. In some cases of suspected pediatric non-accidental trauma, skull radiographs are still performed as part of a skeletal survey in addition to CT, however this does not supplant the need for CT when TBI is clinically suspected. Although radiographs may help differentiate accessory sutures from fractures, this too may become obsolete as three-dimensional skull reformats are increasingly available in clinical practice[14]. In addition, the current CT “scout” view may often serve as a pseudo-radiograph. Transfontanel ultrasound can detect some superficial lesions in neonates such as extra-axial hemorrhage (Figure 1) and has some advocates[15], but is limited by a number of blind spots including parenchymal, posterior fossa and peripheral extra-axial lesions[16] and does not generally have a role in head trauma evaluation[12].

Roles for CT and MR imaging

Acute Moderate and Severe TBI—Rapid imaging helps differentiate patients who require urgent/emergent neurosurgical intervention from those who can be safely monitored or sent home. Noncontrast multi-detector CT (MDCT) has become the consensus choice[11, 17] for the initial imaging study after acute moderate to severe TBI because it is fast, ubiquitous, very sensitive to calvarial injury and radio-opaque foreign bodies (e.g., gunshot fragments), and it is highly accurate for detecting injuries requiring emergent neurosurgical attention--namely hemorrhage, herniation and hydrocephalus. MDCT has also been shown to be useful for predicting clinical outcomes, and the NCCT findings have been incorporated into a number of outcome prediction rules[18-21].

MRI is not typically indicated for the initial evaluation of TBI, as it is less sensitive for fractures, takes longer to acquire, is generally less available, and is relatively expensive as a screening modality. MRI also requires additional safety screening for incompatible medical devices and metallic foreign bodies. However, MRI is exquisitely sensitive to pathologic changes related to even mild TBI (mTBI) and has demonstrated utility for assessing injury severity and prognostication, as discussed in later sections below.

Acute Mild TBI—Mild TBI, as defined by a GCS ≥13, is a misnomer in many cases as patients in this category often experience long-term debilitating symptoms that may interfere

with normal daily activities[22]. Nor does this definition for mTBI imply an absence of structural abnormalities on imaging. In a recent prospective study evaluating imaging features in mTBI patients, Yuh and colleagues identified TBI-CDE-defined pathoanatomic features in 42% of patients when combining results from day-of-injury CT and semiacute MRI[22]. Several guidelines, including the Canadian CT Head Rules[20], New Orleans Criteria[21], and National Emergency X-Ray Utilization Study (NEXUS)-II[19] are routinely employed to identify the cohort of patients who can safely bypass the initial noncontrast CT[18]. When imaging is clinically indicated, noncontrast CT is the primary initial modality of choice for evaluation of acute mTBI [11, 17]. After clinical screening, the majority of patients with mTBI for which imaging is indicated will have normal noncontrast CTs (i.e. "Uncomplicated" mTBI).

Short-term Follow-up Imaging—While MDCT is recommended in patients with neurological deterioration following TBI, studies have shown little benefit for routine follow up imaging[23]. Among patients with initial MDCT positive for intracranial traumatic injury, only certain attributes including subfrontal/temporal hemorrhagic contusion, use of anticoagulation, age over 65 years, and volume of ICH >10 cc have shown high risk for progression[24]. At many institutions it is commonplace to obtain routine follow up MDCT in patients on anticoagulation, even when the initial MDCT is negative for acute intracranial pathology, though the clinical utility of this practice is not well established[25]. One recent prospective study evaluating patients with mild head trauma who were on anticoagulation found that repeat head CT imaging revealed hemorrhagic changes in only 1.4% of such patients after negative initial scan[26].

MRI often plays a complementary role to CT and is most indicated in the acute setting for mTBI when a patient's symptoms and/or neurologic exam are not explained by CT findings. Compared with CT, MRI is far more sensitive for detection of acute traumatic pathology in mTBI, particularly for detection of non-hemorrhagic contusion and traumatic axonal injury (TAI)[27-33]. For these reasons, MRI is also indicated within the first 2 weeks of any moderate or severe TBI for sensitive assessment of the degree of parenchymal injury.

Imaging Subacute/Chronic TBI—Subacute and chronic TBI are best evaluated with MRI[11, 17, 34], which outperforms CT in its ability to identify parenchymal atrophy, white matter injury, and microhemorrhage. Imaging is indicated in patients who experience new, persistent, or worsening symptoms. NCCT should be performed to evaluate subacute/chronic TBI if MRI is contraindicated or unavailable.

Vascular Imaging—Intravenous contrast administration is not necessary or useful in the evaluation of TBI unless arterial or venous injury is suspected. NCCT findings can identify patients at increased risk for traumatic vascular injuries[35]. Patients with skull base fractures, particularly through the carotid canal, have much higher incidence of arterial injuries. Other findings that should raise suspicion for arterial injury include epistaxis, LeFort II and III facial fractures, high cervical spine fractures, GCS ≤8, or TAI[36]. Either CTA or MRA can be performed as an initial screening evaluation for arterial injury[11, 17], though CTA has gained popularity over the past decade with the proliferation of MDCT and the resultant high

quality, 3-dimensional reformats (3D), rapid imaging of contrast bolus[37]. Conventional catheter angiography may be necessary for the diagnosis and treatment of certain lesions.

Venous injury should be suspected in patients with skull fractures extending across adjacent dural venous sinuses. A common injury involves an occipital fracture extending to the underlying transverse sinus (Figure 2). Either CT Venography (CTV) or MR Venography (MRV) are indicated to evaluate for dural venous sinus thrombosis in such cases [11].

Pediatric imaging—Head trauma is a common imaging indication in children and recommended imaging studies largely mirror those recommended for adults for given indications[12]. Children are more susceptible to harmful effects of ionizing radiation than adults and every effort should be made to avoid unnecessary examinations, particularly CT. In balance, however, diagnostic head CT should not be avoided when clinically indicated because of an overemphasized concern for the relatively small radiation dose associated with modern scanners. When CT is performed, dedicated pediatric CT protocols should be used to keep the dose as low as possible (see http://www.imagegently.org for more information). MRI does not expose patients to ionizing radiation; however, it does present its own challenges in pediatric patients. Children may require general anesthesia to tolerate MR examinations, which are much longer and more sensitive to motion than CT. “Rapid” MRI exams with limited sequences and imaging time reduced to 3-4 minutes[38] may help with this in the future, but further studies are required to ensure diagnostic accuracy is on par with CT and standard MR imaging.

IMAGING PROTOCOLS FOR TBI

Optimal neuroimaging protocols for specific head injuries vary depending on individual patient and environmental circumstances. This is particularly true for MR imaging, where there is a greater diversity in choice of available sequences and imaging parameters. It is important to always keep the patient's clinical condition in mind; at times, it is necessary to omit certain sequences in an abbreviated MR examination or substitute CT to shorten the examination time.

Experts in TBI recently convened as part of the “Advanced Integrated Research on Psychological Health and Traumatic Brain Injury: Common Data Elements (CDE)” joint workshop[9]. During this meeting, an expert panel proposed standardized CT and MRI protocols for studying TBI. The panel defined different imaging protocols into a Tier 1 practical clinical imaging protocol and advanced research protocols (Tiers 2 through 4). In this section we describe the Tier 1 clinical imaging protocols. Description of some elements of the Tiers 2 to 4 protocols can be found later in the advanced imaging subsections.

Routine CT protocol

CT imaging is typically acquired helically in the axial plane on a MDCT scanner. An axial slice thickness of 2.5 mm is commonly employed for evaluating the brain parenchyma, though, thinner reformats (0.625 mm) using a bone kernel is recommended for the detection of subtle fractures. Helical acquisition allows the generation of reformatted images in different planes (typically coronal and sagittal), as well as volume rendered 3D reformats,

which can aid in the detection of subtle intracranial hemorrhage and fractures[39, 40]. Modern CT scanners also typically employ dose reduction software, which reduces patient radiation exposure.

Routine MRI protocol

The recommended clinical protocol (Tier 1) tailored for TBI evaluation (Table 2) incorporates multiplanar T1-weighted images (T1WI) (3D T1 if available), T2-weighted images (T2WI) (at 3T, 3D T2 is recommended if available), T2-FLAIR weighted, and T2*-weighted gradient-recalled echo (GRE) or susceptibility weighted (SWI) sequences, in addition to standard diffusion weighted imaging (DWI). SWI sequences are rapidly being added to routine TBI imaging protocols are preferred over GRE due to their increased sensitivity for blood products [41]. Detection, localization and characterization of traumatic lesions benefit from the incoporation of multiple imaging planes, an advantage of 3D acquisitions [9, 27, 29, 30, 32]. Multiplanar imaging is particularly helpful in detecting small lesions (e.g., traumatic brainstem injury) which can be missed due to partial volume averaging effects or an interslice gap [30].

Attributes of particular sequences for imaging specific pathologies will be covered in detail in the sections below. Briefly, T1WI is commonly employed to map brain anatomy while T2WI is sensitive to pathology. Increased water content, as seen in cerebral edema, manifests as T2 prolongation and increased T2 signal intensity. 3D T1 sequences can be utilized for quantitative volumetric analysis of the brain (usually in research settings)[42].

FLAIR T2WI increases the conspicuity of lesions adjacent to, and within, the ventricles and subarachnoid spaces by supressing CSF signal, which is normally bright on T2WI. GRE images and SWI sequences take advantage of artifacts associated with blood products to identify hematomas by their distinctive areas of magnetic susceptibility-induced hypointensity arising from paramagnetic iron.

DWI measures the freedom of molecular motion of water in tissue and is useful in identifying pathologic lesions including foci of axonal injury and infarction[43, 44]. DWI is best used in conjunction with its associated ADC map which can distinguish between cytotoxic and vasogenic edema in the acute and subacute phases and is highly sensitive in the detection of secondary acute ischemic infarction associated with TBI.

Postcontrast T1WI is not recommended as part of routine TBI MRI protocol as it does not improve sensitivity for TBI lesions[9]. Postcontrast imaging can be employed as an optional sequence in certain situations, such as establishing chronicity of injury, subacute ischemia, or when non-traumatic intracranial pathologies are under consideration[45].

IMAGING FINDINGS OF TRAUMATIC BRAIN INJURIES

Intracranial pathology can be subdivided to anatomic location, the most basic distinction being whether it localizes to the brain parenchyma (intra-axial) or outside the brain tissue (extra-axial). Vascular injuries, while typically extra-axial, are addressed separately in this discussion to highlight differences in the imaging workup.

Extra-axial lesions

Three intracranial, extra-axial spaces—epidural, subdural, and subarachnoid spaces—are potential sites for posttraumatic pathology, most often hemorrhage. . NCCT is excellent at detecting acute hemorrhage, which appears hyperdense to the surrounding brain parenchyma typically measuring between 50 and 70 Hounsfield units. In general, the density of a hematoma decreases as it ages, which can create challenges for identifying subacute and chronic hemorrhages that may appear isodense to the surrounding brain parenchyma.

While initially thought to be less sensitive than CT for acute hemorrhage, modern MRI now outperforms CT in identifying hemorrhage throughout all stages of its evolution, particularly small, subacute bleeds[29, 46]. Additionally, due to biochemical changes in hemoglobin over time that alter T1 and T2 relaxation times in hematoma, the age of hemorrhage can be estimated with MRI (Table 3)[46].

Epidural hematoma—Epidural hematomas (EDH) form as blood collects in the potential spaces between the inner table of the skull and the dura. EDHs can be arterial or venous in origin, and may relate to direct bleeding from fractured bone into the epidural space. Arterial epidural hematomas most commonly arise from laceration of meningeal arteries--typically the middle meningeal artery in the temporal or temporoparietal region[47-52]. In adults, an overlying skull fracture is present in the vast majority of cases. Occasionally (9%), EDHs can occur from stretching and tearing of meningeal arteries in the absence of fracture. The latter occurs commonly in children due to transient deformation and depression of the calvarial vault[47].

EDHs classically appear as a lenticular-shaped hematoma, which can cross dural attachment sites, but cannot cross cranial sutures (Figure 3). On CT, acute EDHs generally appear hyperdense. Some hematomas can appear heterogeneous with intrinsic irregular areas of low density, termed the “swirl sign,” an important imaging finding that corresponds to extravasation of hyperacute unclotted blood[53]. EDHs with this sign tend to rapidly expand and warrant urgent surgical consultation. Rarely, it may be difficult to differentiate a small EDH that does not have the classic shape from a subdural hematoma (SDH) on CT. On MRI, the dura mater can often be visualized as a thin line of low signal intensity displaced away from the inner table of the skull, confirming the diagnosis of an EDH[29, 30].

Venous EDHs are less common than those of arterial origin[47-52]. They typically are caused by laceration of a dural sinus in conjunction with fracture of the overlying skull[52, 54]. The posterior fossa (transverse or sigmoid sinus injury), middle cranial fossa (sphenoparietal sinus) (Figure 3G-I), and parasagittal region (superior sagittal sinus) are the most common locations for venous EHD[54]. Venous EDHs, unlike SDHs, are not bound by dural attachments and will often extend both above and below the tentorium. Posterior fossa EDHs occur less frequently (2-29%), are more likely to be of venous origin (85%), and are associated with poorer outcomes than supratentorial lesions[47, 55, 56]. Differentiation of arterial and venous EDHs is usually possible with MR and may have some therapeutic and prognostic significance as venous EDH typically do not progress as rapidly as arterial EDH[52]. Venous EDH may exhibit a more variable shape than those of arterial origin[47, 52]. Invariably, venous EDH are found adjacent to a fracture transgressing a dural venous

sinus[47, 55, 56]. These injuries have a high rate of associated dural sinus thrombosis or occlusion[51] . When in question, patency of the sinus can usually be established by CTV or MRV. When evaluating for venous sinus injury, it is important to distinguish external sinus compression by epidural blood from traumatic venous sinus thrombosis. In the latter, the dural venous sinus is usually irregular with a central sinus filling defect correlating to the thrombus.

Subdural hematoma—Within the skull, the brain is relatively mobile and can move relative to the fixed dural sinuses. Injury to the bridging veins that traverse the subdural space connecting the brain to the dural sinuses results in the SDH[57-59]. While SDHs are most often found along the supratentorial convexities, they can also occur in the posterior fossa, along the falx cerebri, and adjacent to the tentorium[60, 61]. Interhemispheric and tentorial leaf SDH are common in children, including cases of abuse resulting from violent shaking (shaken-baby syndrome)[62-65]. Although these hematomas are not specific for child abuse, their presence should lead to close consideration of the possibility.

Most SDHs manifest as a crescentic collection between the brain and the or inner table of the skull; interhemispheric and tentorial SDHs have a more linear morphology. All SDHs follow the typical appearance of evolving blood on CT and MR (Figure 4). While large acute hyperdense SDHs are readily apparent on CT, small subacute SDHs are often isodense and can be difficult to identify (Figure 4C). MR has been shown to be considerably more sensitive than CT for detection of SDH[29, 30, 66] and the MR signal characteristics varies predictably with the age of the lesion (Table 3). SDHs appear much more conspicuous on MR due to high imaging contrast between the hematoma and signal void of the adjacent cortical bone (Figure 4E). Fortunately, SDHs not identified with CT almost always measure only 1 to 2 mm in diameter and are of doubtful clinical significance[29]. MR also more clearly reveals the multicompartmental nature of subacute to chronic SDH, which can help establish the age of lesions and aid in planning for surgical drainage of these complex lesions[27].

Subarachnoid and Intraventricular Hemorrhage—Subarachnoid hemorrhage (SAH) is a common finding in TBI. One large European series found evidence of SAH in 40% of patients with moderate-severe head injury[67, 68]. Traumatic SAH is also the most common isolated finding in cases of mTBI and has been associated with poor outcome scores at 3 months after injury[22]. Acute traumatic SAH results from injury to small subarachnoid vessels or extension of intraparenchymal hemorrhage beyond the pial limiting membrane and into the subarachnoid space. Traumatic pseudoaneurysms typically do not occur in the acute setting.

Acute SAH appears as curvilinear hyperdensity within the cortical sulci, sylvian fissures and basal cisterns on NCCT (Figure 5F). Historically, SAH was considered far more difficult to detect with conventional MR than with CT[69, 70]; however, more recent technical improvements and additional sequences have shown MRI to be sensitive to SAH and hold some advantages over CT. FLAIR sequences are highly sensitive to SAH (Figure 5C) in both acute and subacute periods[71-73], whereas CT sensitivity falls sharply after the first few days[74]. CSF FLAIR signal hyperintensity is strongly suggestive of hemorrhage after trauma, although other processes that lead to increased CSF protein/cellularity such as infection and

leptomeningeal carcinomatosis may have a similar appearance[75]. The combination of FLAIR and SWI sequences gives MRI (Figure 5) a better detection rate for SAH than NCCT[76].

Intraventricular hemorrhage (IVH), considered a type of intra-axial injury by some authors, is addressed here because its pathophysiology and imaging findings largely overlap with SAH. IVH is also common in patients with head injury, occurring in from 3% to 35% of cases, depending on the severity of trauma[27, 28, 30, 60]. Primary IVH may be caused by a variety of traumatic lesions including TAI, intracerebral hematoma (ICH), and contusions[27, 28, 30, 60]; however, the most prevalent etiology is thought to be the tearing of subependymal veins by rotational strain[31]. Similar rotational forces are thought to cause callosal TAI and, indeed, one published series identified IVH in 60% of patients with TAI of the corpus callosum, but in only 12% of patients without callosal injury[31]. Interestingly, another study found that the presence of IVH on admission NCCT was the only CT imaging finding predictive of grade II or III TAI on subsequent MRI[77]. IVH appears similar to SAH with the blood products appearing hyperdense to CSF on CT and hyperintense to CSF on FLAIR and T1WI with MRI[28]. A CSF-blood fluid level is often seen layering within the posterior aspect of the occipital horns (remember that the images are acquired with the patient in the supine position). Because the subarachnoid and intraventricular CSF spaces communicate, delayed imaging may demonstrate IVH due to recirculation of SAH and vice versa.

CSF leak—CSF leak is a complication in approximately 1-3% of TBI cases[78] and is typically associated with a basilar skull fracture. These cases usually present with CSF rhinorrhea (~80%) or otorrhea (~20%) within the first 48 hours after traumatic injury, though cases can present months to years after the initial insult with meningitis or orthostatic headaches[78, 79]. CSF rhinorrhea or otorrhea should prompt the search for a skull base fracture on thin section maxillofacial or temporal bone CT[11]. Common fractures involve of anterior cranial fossa (especially the frontal sinus or cribriform plates), sella and sphenoid sinus, and temporal bone[78].

CT cisternography is rarely used for initial evaluation, but can be helpful for problem solving in patients with multiple skull defects, negative initial CT imaging, or to confirm a CSF fistula when the diagnosis is unclear. In this setting, intrathecal contrast media is injected to opacify the CSF spaces. A positive study shows abnormal increased attenuation within a paranasal sinus, nasal cavity or middle ear secondary to contrast passage through the skull base defect[80].

Cisternography can also be performed as a nuclear medicine study, most commonly with In-111 DTPA. Positive studies show accumulation of tracer in the nasal cavity. While radionucleotide cisternography lacks the anatomic specificity of CT, it can be useful in certain difficult cases, particularly when combined with endoscopic placement of nasal pledgets. The pledgets are removed 24 hours after radionucleotide injection and activity associated with each pledget is counted to evaluate for occult CSF leak [81].

MRI can be performed to assess for possible encephalocele or meningoencephalocele[11]. Some authors have advocated routinely obtaining MRI when CT shows complete or lobular, nondependent opacification of a sinus cavity adjacent to a bony defect because brain parenchymal herniation can be challenging to differentiate from sinonasal secretions on CT[78]. MRI can also show secondary signs of intracranial hypotension resulting from a chronic CSF leak including diffuse pachymeningeal enhancement, subdural collections, “sagging” brainstem and prominence of the dural sinuses and pituitary[79].

Intra-axial injury

Intra-axial injuries refer to lesions within the brain parenchyma. Primary traumatic intra-axial lesions include the cortical contusion, intracerebral hematoma, TAI and brain stem injury. There are also secondary intra-axial injuries that can occur as a result of brain swelling and ischemia. While CT and MR are both quite sensitive for identification of extra-axial traumatic injury, MRI has a dominant role in evaluation of intra-axial pathology, as non-hemorrhagic and very small lesions can be occult on CT.

Parenchymal Contusion—Parenchymal contusions (Figure 7) occur when the brain forcibly impacts the irregular surface of the overlying skull, which typically occurs at (coup injury) or opposite (contrecoup) the site of blunt trauma. Contusions frequently are multifocal and bilateral, usually involving the superficial grey matter. They typically occur in the temporal (46%) and frontal (31%) lobes. These injuries tend to occur immediately adjacent to the petrous bone and posterior to the greater sphenoid wing in the temporal lobe and just superior to the cribriform plate, orbit roof, planum sphenoidale, and lesser sphenoid wing in the frontal lobe[9, 28, 82]. Contusions less often involve the parietal and occipital lobes (13%) and cerebellum (~10%)[28]. Contusions frequently contain hemorrhagic foci ranging in size from punctate cortical surface petechiae to much larger confluent regions of hemorrhage occupying an entire lobe.

Intracerebral Hematoma—Intracerebral hematomas (ICH) (Figure 8) result from injury to intraparenchymal arteries or veins secondary to rotational strain or penetrating trauma[27, 83-85] and are usually located in the fronto-temporal white matter[48] or basal ganglia[83-85]. Differentiation from hemorrhagic contusions or TAI can be challenging[83-85]; ICHs collect between relatively intact parenchyma in contrast to hemorrhagic contusions wherein hemorrhage is within a larger area of injured edematous brain[27]. Prognosis of isolated ICH is generally good[61], but worsens when the lesion coexists with marked mass effect, TAI, or multiple basal ganglia hemorrhages[83, 84]. Temporal lobe hematomas are especially unpredictable, because even a relatively small lesion can lead to uncal herniation. When CTA is also performed, the “spot sign”, or active extravasation of contrast into the hematoma, predicts future expansion of the hematoma and worsens clinical outcome[86, 87].

Traumatic Axonal Injury—Traumatic axonal injury (TAI) is one of the most common and important types of primary injury found in patients with all grades of head trauma. TAI typically results from rotational strain, and manifests as scattered, often bilateral, small white matter lesions with or without hemorrhagic components[9]. When there are greater than

3 foci of radiographically evident TAI involving at least two separate lobes of the brain and the corpus callosum, the term diffuse axonal injury (DAI) is used.

TAI tends to be multifocal. The severity of injury worsens as involvement of the deep anatomic structures become affected[88-90]. In the Adams Classification for TAI, Grade 1 injuries involve the lobar white matter, particularly the grey-white junction frontal and temporal lobes (Figure 9A-D). Grade 2 injuries extend to involve the corpus callosum, particularly the splenium (Figure 9E-H). Grade 3 injuries (Figure 10) involve the dorsolateral aspect of the upper brainstem[88-90].

TAI lesions are usually ovoid with their long axis oriented in the direction of the involved axonal tracts. They range in size from 2 to 15 mm--peripheral lesions tending to be smaller than more central ones. Overall, CT has poor sensitivity for TAI. Only about 10% of TAI display the classic CT findings of punctate hemorrhage (Figure 9) in the characteristic white matter loci[91].

MRI has increased sensitivity for TAI compared with CT[33, 92, 93]. Hemorrhagic TAI appear as foci of increased magnetic susceptibility on GRE and SWI sequences in the characteristic white matter locations(Figure 9). FLAIR imaging may demonstrate foci of hyperintense signal for both hemorrhagic and non-hemorrhagic TAI. Acute TAI lesions display reduced ADC values on DWI (Figure 9), a finding that is equal in sensitivity to FLAIR[94]. MRI may be also a useful prognostic tool. Several recent studies have shown a strong correlation between the burden of TAI lesions and worse clinical outcomes[33, 95, 96].

Brain Stem Injury—Brainstem injury (BSI) can be divided into primary injuries that result directly from the initial impact and secondary injuries which develop subsequently[30, 97-99]. Primary brainstem injury can be divided into 4 categories. The first type occurs when severe posterior displacement of the brain forces the dorsolateral upper brainstem to directly impact the tentorium producing laceration or contusion[100]. This mechanism is thought to be uncommon and, unlike brainstem TAI, it is not necessarily associated with more diffuse white matter injury.

The other types of BSI are indirect, the most common of which is brainstem TAI[57, 101]. Brainstem TAI (Figure 11) is invariably seen in the context of similar axonal lesions in the supratentorial white matter[88-90]. A third type of primary BSI is characterized by multifocal scattered petechial hemorrhages concentrated in the deep central white matter, hypothalamus, thalamus, and periaqueductal rostral brainstem[88-90, 102]. These lesions usually carry a grim prognosis[88-90]. While both entities share a shear-strain etiology, unlike brainstem TAI, this entity is not associated with lobar white matter, corpus callosum, or superior cerebellar peduncle lesions[88-90]. It is worth noting that distribution of these petechial hemorrhages differs from the secondary (Duret) hemorrhages described below. The final type of primary BSI is pontomedullary separation or rent, which is caused by a hyperextension-induced tear of the ventral brainstem at the pontomedullary junction[88-90, 103, 104]. This injury may range from an incomplete tear to complete brainstem avulsion and is typically[104], but not invariably[103] fatal.

BSI is usually non-hemorrhagic making visualization with CT difficult[28, 30]. The bulk of our knowledge about these entities has been derived from autopsy studies; however, MRI has allowed evaluation of BSI in non–fatally injured patients[30]. MRI studies have shown that BSI is linked to poor clinical outcomes; dorsal hemorrhagic lesions and the bilateral BSI were particularly strongly associated with poor outcomes[105]. Interestingly, BSI is not universally associated with poor outcomes, as nearly one third of patients with MRI evidence for BSI actually had a good clinical outcome. Non-hemorrhagic lesions were the best predictor for benign clinical course[105].

Secondary Injuries

Much of the morbidity and mortality associated with TBI relates to secondary injuries. Mass effect from hematoma or cerebral swelling in a fixed intracranial volume causes increased intracranial pressure and can lead to herniation. Herniation refers to the displacement of brain parenchyma into a different compartment. Subfalcine herniation (Figure 11A) occurs when the cingulate gyrus is displaced beneath the free edge of the falx cerebri. It can lead to further complications including distal anterior cerebral artery (ACA) territory infarcts[106] (the callosomarginal branch runs along the cingulate sulcus) and contralateral hydrocephalus secondary to obstruction of the foramen of Monro. Uncal herniation (Figure 12) occurs when downward pressure forces the medial temporal lobes to descend below the tentorial incisura into the ambient cistern where they compress the brainstem or posterior cerebral artery (PCA)[107]. Mass lesions or edema in the posterior fossa can result in upward herniation of the superior cerebellum through the incisura and compress the superior cerebellar arteries (SCA). Increased pressure from above can force the cerebellar tonsils inferiorly into the foramen magnum causing mass effect on the medulla and compression of the posterior inferior cerebellar arteries (PICA).

Downward transtentorial herniation can lead to BSI secondary to mechanical compression. Duret hemorrhages (Figure 12B,C) are typically centrally located collections of blood in the tegmentum of the rostral pons and midbrain associated with a grim prognosis[30, 88-90, 102, 108-110]. These secondary brainstem hemorrhages are thought to result from stretching/tearing of upper brainstem penetrating arteries during sudden downward transtentorial herniation[30, 102, 109, 110]. Focal brainstem infarcts may also occur via the same mechanism[30, 102, 111].

Both CT and MR are excellent at evaluating for herniation and hydrocephalus, though MR performs better in the posterior fossa where CT is limited by beam hardening artifact[82]. Signs of herniation include midline shift, effacement of the basilar cisterns and cerebral sulci, and (often contralateral) ventricular entrapment[112].

Hypoxic-ischemic brain injury typically results from a period of catastrophic cardiac or vascular compromise. On imaging it is associated with diffuse cerebral swelling and edema. Classic CT signs include the grey-white reversal sign[113](i.e., the white matter appears denser than the grey matter) and pseudo-subarachnoid hemorrhage[114] (i.e., the perimesencephalic and sylvian cisterns appear hyperdense to brain; the falx and tentorium also appear abnormally hyperdense). On MRI, the earliest imaging abnormality is reduced diffusion, particularly in the cerebral cortex, cerebellar hemispheres and basal ganglia[115]. Diffuse

hypoxic-ischemic BSI usually occurs in conjunction with supratentorial ischemic injury. Brainstem involvement is usually a late event as the brainstem is usually spared until just prior to death[30].

Vascular Injury

Traumatic arterial injury can result from several mechanisms including laceration by fracture fragments, blunt or penetrating trauma, vascular compression from brain herniation as mentioned above, and arterial strain[27, 116-118]. Intracranial internal carotid artery and vertebral segments are much less likely to suffer injury than the cervical segments[119]. Skull base fractures are among the most common causes of arterial injury—the presence of basilar fractures on NCCT should always prompt consideration of CTA or MRA for further evaluation[116]. Conventional angiography may be necessary in some cases, particularly when the lesion is subtle or endovascular therapy is the treatment of choice (e.g., severe hemorrhage, epistaxis, or carotid-cavernous fistula).

Arterial Dissection—Dissection occurs when damage to the arterial intima allows blood products to accumulate within the vessel wall (intramural hematoma) which may narrow or occlude the lumen[116]. The intracranial internal carotid arteries are most vulnerable to fracture-related dissections and occlusions adjacent to the anterior clinoid process and clino-carotid canal[35, 116, 117, 120, 121]. Carotid injury in this region is associated with high incidence of concurrent traumatic optic nerve injury and vice versa, so injury to one of these structures should prompt increased attention to the other[27, 35]. Injuries of the vertebral arteries are also frequently encountered, producing a similar spectrum of injuries as seen with the carotid arteries[116]. These most commonly include traumatic dissection, laceration, and arteriovenous fistula[116].

On CTA and MRA sequences, arterial dissection (Figure 13) can be identified by eccentric narrowing of the vascular lumen with an overall slight increase in the external diameter of the artery[119]. The addition of thin (<3 mm) T1WI with fat-saturation to highlight T1-shortening (beginning 48 hours after injury) within the subacute intramural hematoma can be helpful to establish definitive vessel occlusion or dissection, which may obviate the need for catheter angiography[35]. MRI with DWI is also excellent at identifying associated cerebral infarction related to distal emboli or decreased cerebral perfusion.

Traumatic Pseudoaneurysm—Pseudoaneurysms occur when a tear in the inner wall of a vessel is covered by an intact outer adventitial layer[35, 116, 117, 120-122]. These false aneurysms can develop gradually over a period of a few weeks to a few years. Symptoms, if any, are usually related to suprasellar mass effect causing vision changes and cranial neuropathies, epistaxis, or intermittent ischemic events due to embolization of clot[35, 116, 117, 120, 121]. On NCCT, pseudoaneurysms appear as hyperdense round masses adjacent to vessels, but they may also have a somewhat irregular morphology (Figure 14). Appearance of a nonacute pseudoaneurysm on MR may vary, but generally it can be identified by concentric laminated rings of hemorrhage in various stages of evolution[35]. A patent vessel lumen can usually be recognized by its associated flow void[35]. The tendency of these lesions to present long after trauma can lead to diagnostic confusion; familiarity with

their imaging appearance is important to facilitate rapid intervention and prevent potentially catastrophic biopsy of these pseudotumors.

Carotid-Cavernous Fistula—The carotid-cavernous fistula (CCF) is an arterio-venous fistula (AVF) that results from a full-thickness arterial tear of the ICA located within the cavernous sinus. This allows high pressure arterial blood direct access into the low pressure cavernous sinus venous system[35, 116, 118, 123]. The CCF can be divided into direct and indirect types based on arterial supply. The direct CCF, as the name implies, features direct communication between the cavernous ICA and cavernous sinus. In the indirect CCF, connection between the carotid system and the cavernous sinus usually occurs via small branches of the ECA or extracavernous ICA. Nearly all direct CCFs occur secondary to trauma, while indirect CCF are much more likely to be non-traumatic.

The imaging appearance of the CCF depends the amount of flow shunted and the patients venous collateral anatomy. “High flow” lesions are suggested on CT and MR imaging by enlargement of the ipsilateral cavernous sinus and surrounding venous structures such as the superior ophthalmic vein and petrosal sinuses[116]. On a properly timed CTA, asymmetric early enhancement of the affected cavernous sinus and its draining veins may also be noted[124]. On MRI, abnormal flow voids connoting rapid flow may be seen within these enlarged draining veins [118, 121], and abnormal flow-related enhancement may be noted on MRA. Proptosis, extraocular muscle enlargement,stranding of the retro-orbital fat, and orbital preseptal soft tissue swelling may be identified because of elevated capillary and venous pressure. Bilateral enlargement of the superior ophthalmic veins is a classic finding indicating free communication of the fistula through the cavernous plexus of veins[116]. However, when the fistula drains predominately via the inferior petrosal sinus, the superior ophthalmic vein may not be abnormally enlarged. Less common “low flow” CCFs occur when the arterial source is a small calibler intracavernous branch of the ICA rather the cavernous ICA itself. Cross-sectional imaging findings may be much less obvious in these cases and conventional arteriography may be required for definitive diagnosis and potential endovascular treatment.

Dural Arteriovenous Fistula—Dural arteriovenous fistulas are rarely traumatic in etiology, though they can occur when an injured artery forms a connection with an adjacent draining vein or venous sinus. Most case reports in the literature involve a skull fracture that lacerates the middle meningeal artery and its associated venae comitantes[125, 126]. These patients may not develop an EDH as would be expected with middle meningeal artery injury because the arterial extravasation evacuates through a dural (meningeal artery-to-meningeal vein) fistula. These injuries may remain asymptomatic or come to attention during workup for tinnitus months later because of increased flow through the petrosal sinuses and internal jugular vein. Contrast enhanced CT and conventional MR findings in these cases are usually limited to venous distension.

Arterial Spin Labelling (ASL) is a promising, relatively new, advanced MRI technique used to measure cerebral perfusion. ASL electromagnetically tags arterial blood water proximal to the brain which is used as a diffusible tracer to quantify blood flow. Typically, the labelling signal degrades before tagged water molecules can pass through the capillary bed

into draining veins; however, in an AVF, the capillary bed is bypassed by the fistula connecting the artery directly to the vein. Therefore, the presence of ASL signal within venous structures should raise concern for an AVF. Indeed, one recent study found that inclusion of ASL sequences may improve sensitivity for small AVFs[127].

Cerebral Fat Embolism Syndrome (CFES)—Co-morbid long bone fractures are not infrequent with TBI polytrauma. The exact pathogenesis of cerebral fat emboli is controversial, but one favored hypothesis is traumatic introduction of bone marrow fat into the systemic and pulmonary circulations. Neurologic symptoms may include focal neurological signs or generalized encephalopathy which can range from drowsiness to coma[128]. The imaging manifestations are best appreciated on MRI as patchy or confluent regions of vasogenic edema involving deep white matter, basal ganglia, corpus callosum, and cerebellar hemispheres[129-131]. In addition, due to the embolic phenomenon, cytotoxic injury with reduced diffusion has been described[132]. As a manifestation of CFES, a diffuse pattern of multiple micro-susceptibility lesions may be observed on GRE or SWI sequences related to microhemorrhage and/or secondary vascular stasis with increased intravascular deoxyhemoglobin content and microthrombi formation (Figure 15). The MRI appearance may mimic that of TAI, which often coexists. Distinguishing between these two considerations may have both management and prognostic implications[132]. Importantly, while TAI is present immediately after injury, CFES usually occurs in a slightly delayed fashion 48-72 hours after injury[133], and is often associated with the characteristic pulmonary and cutaneous manifestations of CFES. On imaging, hemorrhagic TAI is usually irregular in size and distribution, with clustered foci of axonal injury in characteristic locations (juxtacortical, splenium, dorsal pons and midbrain), while lesions related to CFES are more symmetric, uniform, and diffuse in appearance, consistent with a mechanism of cardio-embolic showering. In addition, TAI is relatively uncommon in the cerebellum, whereas it is a common location for CFES. The role of advanced imaging techniques such as DTI for characterising CFES is an area of active investigation.

ROLE OF ADVANCED IMAGING TECHNIQUES

Advanced imaging techniques are areas of active research and development and are currently targeted to two main areas: evaluating mTBI and obtaining prognostic information for all levels of TBI severity. While promising, these techniques are limited for current clinical applications[37]. Presently, none of these advanced MR techniques are recommended by the American College of Radiology (ACR) appropriateness guidelines for routine evaluation of the TBI patient[11]. Nevertheless, familiarity with these modalities and their application is worthwhile as they may benefit subsets of current patients and will likely be increasingly utilized in the future.

Diffusion Tensor Imaging

The discovery that diffusion of water molecules in cerebral white matter is directionally dependent (anisotropic), with the favored direction of diffusion parallel to the direction of axonal tracts in the brain, laid the foundation for diffusion tensor imaging (DTI) in the brain[134]. These properties have led to a great deal excitement for DTI as a potential

biomarker for white matter pathology, including TBI[135]. DTI builds upon conventional DWI by adding the ability to determine the 3D directionality and magnitude (tensor) of water motion. This is accomplished by acquiring at least 6 (but usually many more) non-collinear diffusion gradient directions. DTI can quantify diffusion using a variety of parameters, the most common of which are fractional anisotropy (FA), which quantifies the degree of anisotropy within a voxel, and mean diffusivity (MD), which quantifies the average magnitude of diffusivity over all sampled directions.

A complete review of the DTI literature related to TBI is beyond the scope of this article—for greater depth, there are a number of excellent reviews recently published on this topic[135-137]. To date, attempts to make generalizable conclusions about DTI in TBI in a single individual have been hindered by heterogeneity in study design with respect to patient populations, imaging parameters, analysis techniques and imaging time points[135]. While most studies of TBI have reported increases in MD and decreases in FA in areas of injury[138-146], studies of acute/semiacute TBI can also be found in literature that report affected white matter FA values that are normal[147] and/or decreased[22, 148] relative to normal controls. In part, these discrepancies likely reflect the intrinsic heterogeneity of TBI, though they also highlight the need for larger studies with standardized imaging and analysis protocols as well as consistent and proper outcome measures[135].

“Group analyses” of TBI patients have validated DTI as a robust measure of TAI at that level[136]. These studies have found abnormal MD and FA frontal and temporal lobe association areas that correlate with behavioural and cognitive outcome measures at follow-up[22, 141, 149]. A recent study of mTBI patients by Yuh and colleagues[22] demonstrated that the prognostic utility of DTI parameters surpassed CT, clinical, demographic, and socioeconomic variables as predictors of 3 and 6 month outcome at both group and individual patient levels. Such studies highlight the potential of DTI for diagnostic and prognostic purposes in individual patients and may soon lead to consensus guidelines for utilization of DTI parameters in TBI imaging.

Perfusion Imaging

TBI is associated with impaired cerebrovascular autoregulation, increased permeability of the blood- brain barrier, and vascular injuries, all of which can lead to altered cerebral blood flow, ischemia and even infarction[150]. For these reasons, cerebral perfusion has long been a target for imaging interrogation. Numerous techniques have been employed in the literature including single-photon emission computed tomography (SPECT)[151-154], positron emission tomography (PET)[155], Xenon-enhanced computed tomography (Xe-CT)[156], perfusion CT (CTP)[157], and dynamic susceptibility contrast (DSC)[158], and as mentioned above, arterial spin-labelling (ASL)[159, 160] perfusion MR. Each of these techniques have relative advantages and disadvantages. SPECT and DSC perfusion studies only allow qualitative comparison between regions of the brain[37], while $^{15}O_2$ PET, Xe-CT, CTP and ASL are quantitatively accurate. Xe-CT and $^{15}O_2$ PET require specialized and expensive equipment that is not widely available, and in the case of $^{15}O_2$ the extremely short half-life of ^{15}O (2 minutes).

A large proportion of the current data relating to brain perfusion after TBI is derived from 99mTc-HMPAO SPECT[151-154], Xe-CT and CTP imaging studies[156, 157]. In these studies, regional hypoperfusion correlate with injury severity; favorable outcomes are seen in TBI patients with hyperemia on baseline imaging, while oligemia portends a poor outcome[156, 157]. Of these study types, CTP is the most readily available, however, it requires repeated imaging over a narrow band of skull and does contribute to increased radiation dose.

Fewer studies have evaluated the utility of perfusion-weighted MR techniques in TBI. The most common utilized MR perfusion technique is dynamic susceptibility contrast (DSC) imaging. Using this technique, Garnett and colleagues[158] measured reduced cerebral blood volume (CBV) in areas of contusion, as well as in a subset of patients with normal appearing brain parenchyma. Interestingly, although the sample size in this study was small, reduced CBV was noted on DSC MRI, even in those patients with an otherwise normal MRI, and this correlated with worse clinical outcome[158]. ASL is an alternative MR perfusion technique that does not require intravenous contrast (see technical description above in the Vascular Injury section.) In mTBI patients undergoing ASL imaging, decreased regional cerebral blood flow (CBF) in the thalamus was found to be strongly correlated with neurocognitive impairment[159, 160]. While these studies were underpowered to evaluate prognostic capacity of ASL perfusion in mTBI patients, the findings are enticing. As with other advanced imaging techniques, more prospective and longitudinal studies are needed to determine the role of perfusion imaging for TBI evaluation.

Magnetic Resonance Spectroscopy

Magnetic resonance spectroscopy (MRS) allows for quantification of certain tissue metabolites *in vivo* with standard clinical MR hardware[161, 162]. Most clinically relevant MRS applications use signal from the hydrogen proton (^{1}H) because of its natural abundance within biologic molecules of interest. This technique produces spectra with peaks corresponding to specific metabolites within a prescribed region of interest or voxel. The peaks for particular metabolites have characteristic locations along a spectrum (chemical shift) and their concentrations can be measured as the area under their respective peak.

Spectroscopic analysis can be performed on tissue within a single cubic volume of interest (single-voxel spectroscopy) or within a multivoxel grid placed over a larger region of interest (chemical shift imaging or MR spectroscopic imaging). Commonly measured metabolites in the brain include N-acetyl aspartate (NAA), a marker of neuronal viability; lactate, a marker of anaerobic glycolysis; choline (Cho), a marker of cellular membrane turnover; Creatinine (Cr), a molecule involved in cellular energy utilization; myo-inositol (mI), a marker of membrane turnover and possibly reactive gliosis; and glutamate and glutamine (Glx), markers of excitatory neurotransmission. Creatinine, often used as a denominator to normalize the other peaks, should be interpreted with caution in MRS studies as its concentration can be altered after TBI.

Spectroscopic studies performed shortly after TBI show a consistent imaging pattern manifested by increased Cho and decreased NAA in regions of the adult brain known to be most susceptible to shear injury such as the splenium of the corpus callosum and centrum

semiovale[163, 164]. These metabolic alterations are thought to reflect TAI, particularly when they occur in the absence of visible injury on conventional anatomic imaging[165-168]. Longitudinal studies in patients with mTBI have shown these changes to be transient with normalization of NAA, Cho, and Glx peaks[164]. Interestingly, Cho and mI peaks remain elevated in the chronic stage, which has been attributed to proliferative astrogliosis[169]. For severe TBI, elevated Cho peaks in the parietal white matter, and elevated Glx peaks in the occipital gray matter, 7 days after injury have been shown to have prognostic value with respect to clinical outcome[162, 170]. In children, the presence of abnormal lactate, Cho and NAA are associated with poor long-term neuropsychological outcomes[171, 172]. Evidence correlating MRS findings and mTBI outcomes are more limited. A recent prospective study found that centrum semiovale Cr levels positively correlated with decreased performance on neuropsychiatric metrics assessed 6 months after injury[173]. Clinical applications for MRS in TBI are also limited by significant overlap in spectral changes seen in a number of other brain disorders, lowering its specificity.

Positron Emission Tomography and Single Photon Emission Computed Tomography

PET and SPECT are composed of tracer molecules tagged with radioisotopes and are typically used to image physiologic processes. Early studies employing PET and SPECT in TBI primarily focused on perfusion imaging (described above) and metabolic imaging, primarily with fluorodeoxyglucose (FDG)-PET[174]. While the current clinical utility for these techniques in TBI is limited, they have a great deal of potential[37]. For example, recent studies have shown potential for PET radiotracers targeting tau and amyloid plaques[175, 176], which are known to occur chronic traumatic encephalopathy, a form of chronic TBI. Like most areas of advanced imaging of TBI, these studies involve only small patient numbers and further validation is needed before they can clinically be used routinely.

DISCUSSION

Significant recent advances have been made in the imaging of TBI; still, there is much to improve. Advanced techniques such as DTI, PET and fMRI hold a great deal of potential, and with more clinical validation and larger studies they will likely move from primarily research modalities to routine clinical use. Several specific injuries show particular promise for future innovations. Among these, mTBI and chronic traumatic encephalopathy (CTE) are of interest both because of their high prevalence and their lack of findings on conventional imaging. The ability to glean prognostic information from imaging studies is another promising area of active research. As new neuro-therapeutic options for TBI are introduced, neuroimaging will likely guide which patients will benefit from these agents and also help follow their response to therapy.

REFERENCES

1. Faul, MD.; Xu, L.; Wald, MM., et al. Traumatic Brain Injury in the United States: Emergency Department Visits, Hospitalizations and Deaths 2002–2006. Centers for Disease Control and Prevention, National Center for Injury Prevention and Control; Atlanta (GA): 2010.
2. Menon DK, Schwab K, Wright DW, et al. Position Statement: Definition of Traumatic Brain Injury. Archives of physical medicine and rehabilitation. 91(11):1637–1640. [PubMed: 21044706]

3. Cornelius C, Crupi R, Calabrese V, et al. Traumatic brain injury: oxidative stress and neuroprotection. Antioxidants & redox signaling. 2013; 19(8):836–853. [PubMed: 23547621]
4. Readnower RD, Chavko M, Adeeb S, et al. Increase in blood–brain barrier permeability, oxidative stress, and activated microglia in a rat model of blast-induced traumatic brain injury. Journal of Neuroscience Research. 2010; 88(16):3530–3539. [PubMed: 20882564]
5. Hawryluk, GWJ.; Manley, GT. Chapter 2 - Classification of traumatic brain injury: past, present, and future.. In: Jordan, G.; Andres, MS., editors. Handbook of Clinical Neurology. Vol. 127. Elsevier; 2015. p. 15-21.
6. Lobato RD, Cordobes F, Rivas JJ, et al. Outcome from severe head injury related to the type of intracranial lesion. A computerized tomography study. Journal of neurosurgery. 1983; 59(5):762–774. [PubMed: 6619928]
7. Jennett B, Teasdale G, Braakman R, et al. Predicting outcome in individual patients after severe head injury. Lancet. 1976; 1(7968):1031–1034. [PubMed: 57446]
8. Thurmond VA, Hicks R, Gleason T, et al. Advancing integrated research in psychological health and traumatic brain injury: common data elements. Archives of physical medicine and rehabilitation. 2010; 91(11):1633–1636. [PubMed: 21044705]
9. Haacke EM, Duhaime AC, Gean AD, et al. Common data elements in radiologic imaging of traumatic brain injury. Journal of magnetic resonance imaging : JMRI. 2010; 32(3):516–543. [PubMed: 20815050]
10. Hicks R, Giacino J, Harrison-Felix C, et al. Progress in developing common data elements for traumatic brain injury research: version two--the end of the beginning. J Neurotrauma. 2013; 30(22):1852–1861. [PubMed: 23725058]
11. Vilaas, S.; Shetty, M.; Martin, N.; Reis, M.; Joseph, M.; Aulino, M., et al. [November 18, 2015] ACR Appropriateness Criteria® Head Trauma.. American College of Radiology. https://acsearch.acr.org/docs/69481/Narrative/.
12. Maura, E.; Ryan, M.; Susan Palasis, M.; Gaurav Saigal, M., et al. [November 18, 2015] ACR Appropriateness Criteria® Head Trauma — Child.. American College of Radiology. https://acsearch.acr.org/docs/3083021/Narrative/.
13. Dunning J, Daly JP, Lomas J-P, et al. Derivation of the children's head injury algorithm for the prediction of important clinical events decision rule for head injury in children. Archives of Disease in Childhood. 2006; 91(11):885–891. [PubMed: 17056862]
14. Prabhu SP, Newton AW, Perez-Rossello JM, et al. Three-dimensional skull models as a problem-solving tool in suspected child abuse. Pediatric radiology. 2013; 43(5):575–581. [PubMed: 23184067]
15. Trenchs V, Curcoy AI, Castillo M, et al. Minor head trauma and linear skull fracture in infants: cranial ultrasound or computed tomography? European journal of emergency medicine : official journal of the European Society for Emergency Medicine. 2009; 16(3):150–152. [PubMed: 19425245]
16. Ball WS Jr. Nonaccidental craniocerebral trauma (child abuse): MR imaging. Radiology. 1989; 173(3):609–610. [PubMed: 2813759]
17. Wintermark M, Sanelli PC, Anzai Y, et al. Imaging Evidence and Recommendations for Traumatic Brain Injury: Conventional Neuroimaging Techniques. Journal of the American College of Radiology. 2015; 12(2):e1–e14. [PubMed: 25456317]
18. Ro YS, Shin SD, Holmes JF, et al. Comparison of Clinical Performance of Cranial Computed Tomography Rules in Patients With Minor Head Injury: A Multicenter Prospective Study. Academic Emergency Medicine. 2011; 18(6):597–604. [PubMed: 21676057]
19. Mower WR, Hoffman JR, Herbert M, et al. Developing a decision instrument to guide computed tomographic imaging of blunt head injury patients. The Journal of trauma. 2005; 59(4):954–959. [PubMed: 16374287]
20. Stiell IG, Wells GA, Vandemheen K, et al. The Canadian CT Head Rule for patients with minor head injury. Lancet. 2001; 357(9266):1391–1396. [PubMed: 11356436]
21. Haydel MJ, Preston CA, Mills TJ, et al. Indications for computed tomography in patients with minor head injury. The New England journal of medicine. 2000; 343(2):100–105. [PubMed: 10891517]

22. Yuh EL, Cooper SR, Mukherjee P, et al. Diffusion tensor imaging for outcome prediction in mild traumatic brain injury: a TRACK-TBI study. J Neurotrauma. 2014; 31(17):1457–1477. [PubMed: 24742275]
23. Reljic T, Mahony H, Djulbegovic B, et al. Value of repeat head computed tomography after traumatic brain injury: systematic review and meta-analysis. J Neurotrauma. 2014; 31(1):78–98. [PubMed: 23914924]
24. Washington CW, Grubb RL Jr. Are routine repeat imaging and intensive care unit admission necessary in mild traumatic brain injury? Journal of neurosurgery. 2012; 116(3):549–557. [PubMed: 22196096]
25. Menditto VG, Lucci M, Polonara S, et al. Management of Minor Head Injury in Patients Receiving Oral Anticoagulant Therapy: A Prospective Study of a 24-Hour Observation Protocol. Annals of Emergency Medicine. 59(6):451–455. [PubMed: 22244878]
26. Kaen A, Jimenez-Roldan L, Arrese I, et al. The value of sequential computed tomography scanning in anticoagulated patients suffering from minor head injury. The Journal of trauma. 2010; 68(4): 895–898. [PubMed: 20016390]
27. Gentry LR. Imaging of closed head injury. Radiology. 1994; 191(1):1–17. [PubMed: 8134551]
28. Gentry LR, Godersky JC, Thompson B. MR imaging of head trauma: review of the distribution and radiopathologic features of traumatic lesions. AJR American journal of roentgenology. 1988; 150(3):663–672. [PubMed: 3257624]
29. Gentry LR, Godersky JC, Thompson B, et al. Prospective comparative study of intermediate-field MR and CT in the evaluation of closed head trauma. AJR American journal of roentgenology. 1988; 150(3):673–682. [PubMed: 3257625]
30. Gentry LR, Godersky JC, Thompson BH. Traumatic brain stem injury: MR imaging. Radiology. 1989; 171(1):177–187. [PubMed: 2928523]
31. Gentry LR, Thompson B, Godersky JC. Trauma to the corpus callosum: MR features. AJNR American journal of neuroradiology. 1988; 9(6):1129–1138. [PubMed: 3143234]
32. Yuh EL, Hawryluk GW, Manley GT. Imaging concussion: a review. Neurosurgery. 2014; 75(Suppl 4):S50–63. [PubMed: 25232884]
33. Yuh EL, Mukherjee P, Lingsma HF, et al. Magnetic resonance imaging improves 3-month outcome prediction in mild traumatic brain injury. Annals of neurology. 2013; 73(2):224–235. [PubMed: 23224915]
34. Le TH, Gean AD. Neuroimaging of traumatic brain injury. The Mount Sinai journal of medicine, New York. 2009; 76(2):145–162.
35. Gentry LR. Facial trauma and associated brain damage. Radiologic clinics of North America. 1989; 27(2):435–446. [PubMed: 2645611]
36. Bromberg WJ, Collier BC, Diebel LN, et al. Blunt Cerebrovascular Injury Practice Management Guidelines: The Eastern Association for the Surgery of Trauma. Journal of Trauma and Acute Care Surgery. 2010; 68(2):471–477.
37. Wintermark M, Sanelli PC, Anzai Y, et al. Imaging Evidence and Recommendations for Traumatic Brain Injury: Advanced Neuro- and Neurovascular Imaging Techniques. American Journal of Neuroradiology. 2014
38. Cohen AR, Caruso P, Duhaime AC, et al. Feasibility of “rapid” magnetic resonance imaging in pediatric acute head injury. The American journal of emergency medicine. 2015; 33(7):887–890. [PubMed: 25912791]
39. Wei SC, Ulmer S, Lev MH, et al. Value of Coronal Reformations in the CT Evaluation of Acute Head Trauma. American Journal of Neuroradiology. 2010; 31(2):334–339. [PubMed: 19797789]
40. Zacharia TT, Nguyen DD. Subtle pathology detection with multidetector row coronal and sagittal CT reformations in acute head trauma. Emerg Radiol. 2010; 17(2):97–102. [PubMed: 19809839]
41. Haacke EM, Mittal S, Wu Z, et al. Susceptibility-Weighted Imaging: Technical Aspects and Clinical Applications, Part 1. American Journal of Neuroradiology. 2009; 30(1):19–30. [PubMed: 19039041]
42. Wang X, Xie H, Cotton AS, et al. Early cortical thickness changes after mild traumatic brain injury following motor vehicle collision. J Neurotrauma. 2014

43. Liu AY, Maldjian JA, Bagley LJ, et al. Traumatic brain injury: diffusion-weighted MR imaging findings. AJNR American journal of neuroradiology. 1999; 20(9):1636–1641. [PubMed: 10543633]
44. Huisman TA. Diffusion-weighted imaging: basic concepts and application in cerebral stroke and head trauma. European radiology. 2003; 13(10):2283–2297. [PubMed: 14534804]
45. Lang DA, Hadley DM, Teasdale GM, et al. Gadolinium DTPA enhanced magnetic resonance imaging in acute head injury. Acta neurochirurgica. 1991; 109(1-2):5–11. [PubMed: 2068967]
46. Gomori JM, Grossman RI, Goldberg HI, et al. Intracranial hematomas: imaging by high-field MR. Radiology. 1985; 157(1):87–93. [PubMed: 4034983]
47. Zimmerman RA, Bilaniuk LT. Computed tomographic staging of traumatic epidural bleeding. Radiology. 1982; 144(4):809–812. [PubMed: 7111729]
48. Baykaner K, Alp H, Ceviker N, et al. Observation of 95 patients with extradural hematoma and review of the literature. Surgical neurology. 1988; 30(5):339–341. [PubMed: 3055383]
49. Lobato RD, Rivas JJ, Cordobes F, et al. Acute epidural hematoma: an analysis of factors influencing the outcome of patients undergoing surgery in coma. Journal of neurosurgery. 1988; 68(1):48–57. [PubMed: 3335912]
50. Bricolo AP, Pasut LM. Extradural hematoma: toward zero mortality. A prospective study. Neurosurgery. 1984; 14(1):8–12. [PubMed: 6694798]
51. Servadei F, Faccani G, Roccella P, et al. Asymptomatic extradural haematomas. Results of a multicenter study of 158 cases in minor head injury. Acta neurochirurgica. 1989; 96(1-2):39–45. [PubMed: 2648769]
52. Knuckey NW, Gelbard S, Epstein MH. The management of “asymptomatic” epidural hematomas. A prospective study. Journal of neurosurgery. 1989; 70(3):392–396. [PubMed: 2915245]
53. Al-Nakshabandi NA. The Swirl Sign. Radiology. 2001; 218(2):433–433. [PubMed: 11161158]
54. Gean AD, Fischbein NJ, Purcell DD, et al. Benign anterior temporal epidural hematoma: indolent lesion with a characteristic CT imaging appearance after blunt head trauma. Radiology. 2010; 257(1):212–218. [PubMed: 20713606]
55. Milo R, Razon N, Schiffer J. Delayed epidural hematoma. A review. Acta neurochirurgica. 1987; 84(1-2):13–23. [PubMed: 3548224]
56. Pozzati E, Tognetti F, Cavallo M, et al. Extradural hematomas of the posterior cranial fossa. Observations on a series of 32 consecutive cases treated after the introduction of computed tomography scanning. Surgical neurology. 1989; 32(4):300–303. [PubMed: 2781461]
57. Gennarelli TA, Spielman GM, Langfitt TW, et al. Influence of the type of intracranial lesion on outcome from severe head injury. Journal of neurosurgery. 1982; 56(1):26–32. [PubMed: 7054419]
58. Holbourn AHS. Mechanics of head injuries. Lancet. 1943; 2:438–441.
59. Holbourn AHS. The mechanics of brain injuries. Br Med Bull. 1945; 3:147–149.
60. Cooper, PR. Post-traumatic intracranial mass lesions. 2nd ed. Williams & Wilkins; 1987.
61. Seelig JM, Becker DP, Miller JD, et al. Traumatic acute subdural hematoma: major mortality reduction in comatose patients treated within four hours. The New England journal of medicine. 1981; 304(25):1511–1518. [PubMed: 7231489]
62. Sato Y, Yuh WT, Smith WL, et al. Head injury in child abuse: evaluation with MR imaging. Radiology. 1989; 173(3):653–657. [PubMed: 2813768]
63. Bruce DA, Zimmerman RA. Shaken impact syndrome. Pediatric annals. 1989; 18(8):482–484. 486–489, 492–484. [PubMed: 2671890]
64. Zimmerman RA, Bilaniuk LT, Bruce D, et al. Computed tomography of craniocerebral injury in the abused child. Radiology. 1979; 130(3):687–690. [PubMed: 424539]
65. Cohen RA, Kaufman RA, Myers PA, et al. Cranial computed tomography in the abused child with head injury. AJR American journal of roentgenology. 1986; 146(1):97–102. [PubMed: 3510048]
66. Zimmerman RA, Bilaniuk LT, Grossman RI, et al. Resistive NMR of intracranial hematomas. Neuroradiology. 1985; 27(1):16–20. [PubMed: 3974860]
67. Murray GD, Teasdale GM, Braakman R, et al. The European Brain Injury Consortium Survey of Head Injuries. Acta neurochirurgica. 1999; 141(3):223–236. [PubMed: 10214478]

68. Servadei F, Murray GD, Teasdale GM, et al. Traumatic subarachnoid hemorrhage: demographic and clinical study of 750 patients from the European brain injury consortium survey of head injuries. Neurosurgery. 2002; 50(2):261–267. discussion 267-269. [PubMed: 11844260]
69. Chakeres DW, Bryan RN. Acute subarachnoid hemorrhage: in vitro comparison of magnetic resonance and computed tomography. AJNR American journal of neuroradiology. 1986; 7(2):223–228. [PubMed: 3082153]
70. Bradley WG Jr. Schmidt PG. Effect of methemoglobin formation on the MR appearance of subarachnoid hemorrhage. Radiology. 1985; 156(1):99–103. [PubMed: 4001427]
71. Stuckey SL, Goh TD, Heffernan T, et al. Hyperintensity in the subarachnoid space on FLAIR MRI. AJR American journal of roentgenology. 2007; 189(4):913–921. [PubMed: 17885065]
72. Maeda M, Yagishita A, Yamamoto T, et al. Abnormal hyperintensity within the subarachnoid space evaluated by fluid-attenuated inversion-recovery MR imaging: a spectrum of central nervous system diseases. European radiology. 2003; 13(Suppl 4):L192–201. [PubMed: 15018187]
73. Mitchell P, Wilkinson ID, Hoggard N, et al. Detection of subarachnoid haemorrhage with magnetic resonance imaging. Journal of neurology, neurosurgery, and psychiatry. 2001; 70(2):205–211.
74. van Gijn J, Kerr RS, Rinkel GJ. Subarachnoid haemorrhage. Lancet. 2007; 369(9558):306–318. [PubMed: 17258671]
75. Tha KK, Terae S, Kudo K, et al. Differential diagnosis of hyperintense cerebrospinal fluid on fluid-attenuated inversion recovery images of the brain. Part II: non-pathological conditions. The British journal of radiology. 2009; 82(979):610–614. [PubMed: 19541945]
76. Verma RK, Kottke R, Andereggen L, et al. Detecting subarachnoid hemorrhage: comparison of combined FLAIR/SWI versus CT. European journal of radiology. 2013; 82(9):1539–1545. [PubMed: 23632159]
77. Mata-Mbemba D, Mugikura S, Nakagawa A, et al. Intraventricular Hemorrhage on Initial Computed Tomography as Marker of Diffuse Axonal Injury after Traumatic Brain Injury. J Neurotrauma. 2014
78. Lloyd KM, DelGaudio JM, Hudgins PA. Imaging of Skull Base Cerebrospinal Fluid Leaks in Adults. Radiology. 2008; 248(3):725–736. [PubMed: 18710972]
79. Yuh EL, Dillon WP. Intracranial hypotension and intracranial hypertension. Neuroimaging clinics of North America. 2010; 20(4):597–617. [PubMed: 20974378]
80. Stone JA, Castillo M, Neelon B, et al. Evaluation of CSF leaks: high-resolution CT compared with contrast-enhanced CT and radionuclide cisternography. AJNR American journal of neuroradiology. 1999; 20(4):706–712. [PubMed: 10319986]
81. Glaubitt D, Haubrich J, Cordoni-Voutsas M. Detection and quantitation of intermittent CSF rhinorrhea during prolonged cisternography with 111In-DTPA. AJNR American journal of neuroradiology. 1983; 4(3):560–563. [PubMed: 6410797]
82. Kim JJ, Gean AD. Imaging for the diagnosis and management of traumatic brain injury. Neurotherapeutics : the journal of the American Society for Experimental NeuroTherapeutics. 2011; 8(1):39–53. [PubMed: 21274684]
83. Jayakumar PN, Kolluri VR, Basavakumar DG, et al. Prognosis in traumatic basal ganglia haematoma. Acta neurochirurgica. 1989; 97(3-4):114–116. [PubMed: 2718802]
84. Colquhoun IR, Rawlinson J. The significance of haematomas of the basal ganglia in closed head injury. Clinical radiology. 1989; 40(6):619–621. [PubMed: 2598589]
85. Katz DI, Alexander MP, Seliger GM, et al. Traumatic basal ganglia hemorrhage: clinicopathologic features and outcome. Neurology. 1989; 39(7):897–904. [PubMed: 2739917]
86. Wada R, Aviv RI, Fox AJ, et al. CT angiography “spot sign” predicts hematoma expansion in acute intracerebral hemorrhage. Stroke. 2007; 38(4):1257–1262. [PubMed: 17322083]
87. Park SY, Kong MH, Kim JH, et al. Role of ‘Spot Sign’ on CT Angiography to Predict Hematoma Expansion in Spontaneous Intracerebral Hemorrhage. Journal of Korean Neurosurgical Society. 2010; 48(5):399–405. [PubMed: 21286475]
88. Adams H, Mitchell DE, Graham DI, et al. Diffuse brain damage of immediate impact type. Its relationship to ‘primary brain-stem damage’ in head injury. Brain. 1977; 100(3):489–502. [PubMed: 589428]

89. Adams JH, Graham DI, Murray LS, et al. Diffuse axonal injury due to nonmissile head injury in humans: an analysis of 45 cases. Annals of neurology. 1982; 12(6):557–563. [PubMed: 7159059]

90. Adams JH, Graham DI, Scott G, et al. Brain damage in fatal non-missile head injury. Journal of clinical pathology. 1980; 33(12):1132–1145. [PubMed: 7451661]

91. Meythaler JM, Peduzzi JD, Eleftheriou E, et al. Current concepts: Diffuse axonal injury–associated traumatic brain injury. Archives of physical medicine and rehabilitation. 82(10):1461–1471. [PubMed: 11588754]

92. Mittl RL, Grossman RI, Hiehle JF, et al. Prevalence of MR evidence of diffuse axonal injury in patients with mild head injury and normal head CT findings. AJNR American journal of neuroradiology. 1994; 15(8):1583–1589. [PubMed: 7985582]

93. Orrison WW, Gentry LR, Stimac GK, et al. Blinded comparison of cranial CT and MR in closed head injury evaluation. AJNR American journal of neuroradiology. 1994; 15(2):351–356. [PubMed: 8192085]

94. Kinoshita T, Moritani T, Hiwatashi A, et al. Conspicuity of diffuse axonal injury lesions on diffusion-weighted MR imaging. European journal of radiology. 2005; 56(1):5–11. [PubMed: 16168258]

95. Moen KG, Brezova V, Skandsen T, et al. Traumatic axonal injury: the prognostic value of lesion load in corpus callosum, brain stem, and thalamus in different magnetic resonance imaging sequences. J Neurotrauma. 2014; 31(17):1486–1496. [PubMed: 24773587]

96. Schaefer PW, Huisman TA, Sorensen AG, et al. Diffusion-weighted MR imaging in closed head injury: high correlation with initial glasgow coma scale score and score on modified Rankin scale at discharge. Radiology. 2004; 233(1):58–66. [PubMed: 15304663]

97. Cooper PR, Maravilla K, Kirkpatrick J, et al. Traumatically induced brain stem hemorrhage and the computerized tomographic scan: clinical, pathological, and experimental observations. Neurosurgery. 1979; 4(2):115–124. [PubMed: 440542]

98. Tsai FY, Teal JS, Quinn MF, et al. CT of brainstem injury. AJR American journal of roentgenology. 1980; 134(4):717–723. [PubMed: 6767357]

99. Turazzi S, Alexandre A, Bricolo A. Incidence and significance of clinical signs of brainstem traumatic lesions. Study of 2600 head injured patients. Journal of neurosurgical sciences. 1975; 19(4):215–222. [PubMed: 1232096]

100. Saeki N, Ito C, Ishige N, et al. [Traumatic brain stem contusion due to direct injury by tentorium cerebelli. Case report]. Neurologia medico-chirurgica. 1985; 25(11):939–944. [PubMed: 2421188]

101. Gennarelli TA, Thibault LE, Adams JH, et al. Diffuse axonal injury and traumatic coma in the primate. Annals of neurology. 1982; 12(6):564–574. [PubMed: 7159060]

102. Tomlinson BE. Brain-stem lesions after head injury. Journal of clinical pathology Supplement. 1970; 4:154–165. [PubMed: 4123921]

103. Pilz P. Survival after ponto-medullary junction trauma. Acta neurochirurgica Supplementum. 1983; 32:75–78. [PubMed: 6581708]

104. Britt RH, Herrick MK, Mason RT, et al. Traumatic lesions of pontomedullary junction. Neurosurgery. 1980; 6(6):623–631. [PubMed: 7432604]

105. Hilario A, Ramos A, Millan JM, et al. Severe Traumatic Head Injury: Prognostic Value of Brain Stem Injuries Detected at MRI. American Journal of Neuroradiology. 2012; 33(10):1925–1931. [PubMed: 22576887]

106. Rothfus WE, Goldberg AL, Tabas JH, et al. Callosomarginal infarction secondary to transfalcial herniation. American Journal of Neuroradiology. 1987; 8(6):1073–1076. [PubMed: 3120534]

107. Wernick S, Wells RG. Sequelae of Temporal Lobe Herniation: MR Imaging. Journal of computer assisted tomography. 1989; 13(2):323–325. [PubMed: 2925923]

108. Rosenblum WI, Greenberg RP, Seelig JM, et al. Midbrain lesions: frequent and significant prognostic feature in closed head injury. Neurosurgery. 1981; 9(6):613–620. [PubMed: 7322325]

109. Friede RL, Roessmann U. The pathogenesis of secondary midbrain hemorrhages. Neurology. 1966; 16(12):1210–1216. [PubMed: 5951398]

110. Caplan LR, Zervas NT. Survival with permanent midbrain dysfunction after surgical treatment of traumatic subdural hematoma: the clinical picture of a Duret hemorrhage? Annals of neurology. 1977; 1(6):587–589. [PubMed: 883773]
111. Jellinger K, Seitelberger F. Protracted post-traumatic encephalopathy. Pathology, pathogenesis and clinical implications. Journal of the neurological sciences. 1970; 10(1):51–94. [PubMed: 5411990]
112. Johnson PL, Eckard DA, Chason DP, et al. Imaging of acquired cerebral herniations. Neuroimaging clinics of North America. 2002; 12(2):217–228. [PubMed: 12391633]
113. Han BK, Towbin RB, De Courten-Myers G, et al. Reversal sign on CT: effect of anoxic/ischemic cerebral injury in children. AJR American journal of roentgenology. 1990; 154(2):361–368. [PubMed: 2105031]
114. Given CA 2nd, Burdette JH, Elster AD, et al. Pseudo-subarachnoid hemorrhage: a potential imaging pitfall associated with diffuse cerebral edema. AJNR American journal of neuroradiology. 2003; 24(2):254–256. [PubMed: 12591643]
115. Arbelaez A, Castillo M, Mukherji SK. Diffusion-Weighted MR Imaging ofGlobal Cerebral Anoxia. American Journal of Neuroradiology. 1999; 20(6):999–1007. [PubMed: 10445435]
116. Davis JM, Zimmerman RA. Injury of the carotid and vertebral arteries. Neuroradiology. 1983; 25(2):55–69. [PubMed: 6348583]
117. Goldberg HI, Grossman RI, Gomori JM, et al. Cervical internal carotid artery dissecting hemorrhage: diagnosis using MR. Radiology. 1986; 158(1):157–161. [PubMed: 3940374]
118. Sklar EM, Quencer RM, Bowen BC, et al. Magnetic resonance applications in cerebral injury. Radiologic clinics of North America. 1992; 30(2):353–366. [PubMed: 1535861]
119. Rodallec MH, Marteau V, Gerber S, et al. Craniocervical Arterial Dissection: Spectrum of Imaging Findings and Differential Diagnosis. RadioGraphics. 2008; 28(6):1711–1728. [PubMed: 18936031]
120. Barr HW, Blackwood W, Meadows SP. Intracavernous carotid aneurysms. A clinical-pathological report. Brain. 1971; 94(4):607–622. [PubMed: 5132961]
121. Mokri B, Piepgras DG, Sundt TM Jr. et al. Extracranial internal carotid artery aneurysms. Mayo Clinic proceedings. 1982; 57(5):310–321. [PubMed: 7043107]
122. Edwards JD, Sapienza P, Lefkowitz DM, et al. Posttraumatic innominate artery aneurysm with occlusion of the common carotid artery at its origin by an intimal flap. Annals of vascular surgery. 1993; 7(4):368–373. [PubMed: 8268079]
123. Komiyama M, Hakuba A, Yasui T, et al. Magnetic resonance imaging of intracavernous pathology. Neurologia medico-chirurgica. 1989; 29(7):573–578. [PubMed: 2477754]
124. Coskun O, Hamon M, Catroux G, et al. Carotid-cavernous Fistulas: Diagnosis with Spiral CT Angiography. American Journal of Neuroradiology. 2000; 21(4):712–716. [PubMed: 10782783]
125. Feldman RA, Hieshima G, Giannotta SL, et al. Traumatic dural arteriovenous fistula supplied by scalp, meningeal, and cortical arteries: case report. Neurosurgery. 1980; 6(6):670–674. [PubMed: 7432611]
126. Vassilyadi M, Mehrotra N, Shamji MF, et al. Pediatric traumatic dural arteriovenous fistula. The Canadian journal of neurological sciences Le journal canadien des sciences neurologiques. 2009; 36(6):751–756. [PubMed: 19960755]
127. Le TT, Fischbein NJ, Andre JB, et al. Identification of venous signal on arterial spin labeling improves diagnosis of dural arteriovenous fistulas and small arteriovenous malformations. AJNR American journal of neuroradiology. 2012; 33(1):61–68. [PubMed: 22158927]
128. Jacobson DM, Terrence CF, Reinmuth OM. The neurologic manifestations of fat embolism. Neurology. 1986; 36(6):847–851. [PubMed: 3703294]
129. Citerio G, Bianchini E, Beretta L. Magnetic resonance imaging of cerebral fat embolism: a case report. Intensive care medicine. 1995; 21(8):679–681. [PubMed: 8522674]
130. Stoeger A, Daniaux M, Felber S, et al. MRI findings in cerebral fat embolism. European radiology. 1998; 8(9):1590–1593. [PubMed: 9866767]
131. Takahashi M, Suzuki R, Osakabe Y, et al. Magnetic resonance imaging findings in cerebral fat embolism: correlation with clinical manifestations. The Journal of trauma. 1999; 46(2):324–327. [PubMed: 10029041]

132. Bodanapally U, Shanmuganathan K, Saksobhavivat N, et al. MR imaging and differentiation of cerebral fat embolism syndrome from diffuse axonal injury: application of diffusion tensor imaging. Neuroradiology. 2013; 55(6):771–778. [PubMed: 23515659]
133. Chen PC, Hsu CW, Liao WI, et al. Hyperacute cerebral fat embolism in a patient with femoral shaft fracture. The American journal of emergency medicine. 2013; 31(9):1420, e1421–1423. [PubMed: 23759683]
134. Moseley ME, Cohen Y, Kucharczyk J, et al. Diffusion-weighted MR imaging of anisotropic water diffusion in cat central nervous system. Radiology. 1990; 176(2):439–445. [PubMed: 2367658]
135. Hulkower MB, Poliak DB, Rosenbaum SB, et al. A decade of DTI in traumatic brain injury: 10 years and 100 articles later. AJNR American journal of neuroradiology. 2013; 34(11):2064–2074. [PubMed: 23306011]
136. Niogi SN, Mukherjee P. Diffusion tensor imaging of mild traumatic brain injury. The Journal of head trauma rehabilitation. 2010; 25(4):241–255. [PubMed: 20611043]
137. Shenton ME, Hamoda HM, Schneiderman JS, et al. A review of magnetic resonance imaging and diffusion tensor imaging findings in mild traumatic brain injury. Brain imaging and behavior. 2012; 6(2):137–192. [PubMed: 22438191]
138. Arfanakis K, Haughton VM, Carew JD, et al. Diffusion tensor MR imaging in diffuse axonal injury. AJNR American journal of neuroradiology. 2002; 23(5):794–802. [PubMed: 12006280]
139. Brandstack N, Kurki T, Tenovuo O. Quantitative diffusion-tensor tractography of long association tracts in patients with traumatic brain injury without associated findings at routine MR imaging. Radiology. 2013; 267(1):231–239. [PubMed: 23297328]
140. Kumar R, Gupta RK, Husain M, et al. Comparative evaluation of corpus callosum DTI metrics in acute mild and moderate traumatic brain injury: its correlation with neuropsychometric tests. Brain injury : [BI]. 2009; 23(7):675–685.
141. Miles L, Grossman RI, Johnson G, et al. Short-term DTI predictors of cognitive dysfunction in mild traumatic brain injury. Brain injury : [BI]. 2008; 22(2):115–122.
142. Newcombe VF, Williams GB, Nortje J, et al. Analysis of acute traumatic axonal injury using diffusion tensor imaging. British journal of neurosurgery. 2007; 21(4):340–348. [PubMed: 17676452]
143. Wilde EA, Ramos MA, Yallampalli R, et al. Diffusion Tensor Imaging of the Cingulum Bundle in Children After Traumatic Brain Injury. Developmental neuropsychology. 2010; 35(3):333–351. [PubMed: 20446136]
144. Wozniak JR, Krach L, Ward E, et al. Neurocognitive and neuroimaging correlates of pediatric traumatic brain injury: a diffusion tensor imaging (DTI) study. Archives of clinical neuropsychology: the official journal of the National Academy of Neuropsychologists. 2007; 22(5):555–568. [PubMed: 17446039]
145. Henry LC, Tremblay J, Tremblay S, et al. Acute and chronic changes in diffusivity measures after sports concussion. J Neurotrauma. 2011; 28(10):2049–2059. [PubMed: 21864134]
146. Wilde EA, McCauley SR, Hunter JV, et al. Diffusion tensor imaging of acute mild traumatic brain injury in adolescents. Neurology. 2008; 70(12):948–955. [PubMed: 18347317]
147. Perez AM, Adler J, Kulkarni N, et al. Longitudinal white matter changes after traumatic axonal injury. J Neurotrauma. 2014; 31(17):1478–1485. [PubMed: 24738754]
148. Toth A, Kovacs N, Perlaki G, et al. Multi-modal magnetic resonance imaging in the acute and sub-acute phase of mild traumatic brain injury: can we see the difference? J Neurotrauma. 2013; 30(1):2–10. [PubMed: 22905918]
149. Lipton ML, Gulko E, Zimmerman ME, et al. Diffusion-tensor imaging implicates prefrontal axonal injury in executive function impairment following very mild traumatic brain injury. Radiology. 2009; 252(3):816–824. [PubMed: 19567646]
150. Bigler ED, Maxwell WL. Neuropathology of mild traumatic brain injury: relationship to neuroimaging findings. Brain imaging and behavior. 2012; 6(2):108–136. [PubMed: 22434552]
151. Abu-Judeh HH, Singh M, Masdeu JC, et al. Discordance between FDG uptake and technetium-99m-HMPAO brain perfusion in acute traumatic brain injury. Journal of nuclear medicine : official publication, Society of Nuclear Medicine. 1998; 39(8):1357–1359.

152. Hofman PA, Stapert SZ, van Kroonenburgh MJ, et al. MR imaging, single-photon emission CT, and neurocognitive performance after mild traumatic brain injury. AJNR American journal of neuroradiology. 2001; 22(3):441–449. [PubMed: 11237964]

153. Jacobs A, Put E, Ingels M, et al. Prospective evaluation of technetium-99m-HMPAO SPECT in mild and moderate traumatic brain injury. Journal of nuclear medicine : official publication, Society of Nuclear Medicine. 1994; 35(6):942–947.

154. Davalos DB, Bennett TL. A review of the use of single-photon emission computerized tomography as a diagnostic tool in mild traumatic brain injury. Applied neuropsychology. 2002; 9(2):92–105. [PubMed: 12214827]

155. Yamaki T, Imahori Y, Ohmori Y, et al. Cerebral Hemodynamics and Metabolism of Severe Diffuse Brain Injury Measured by PET. Journal of Nuclear Medicine. 1996; 37(7):1166–1170. [PubMed: 8965189]

156. Rostami E, Engquist H, Enblad P. Imaging of cerebral blood flow in patients with severe traumatic brain injury in the neurointensive care. Frontiers in neurology. 2014; 5:114. [PubMed: 25071702]

157. Wintermark M, van Melle G, Schnyder P, et al. Admission perfusion CT: prognostic value in patients with severe head trauma. Radiology. 2004; 232(1):211–220. [PubMed: 15220504]

158. Garnett MR, Blamire AM, Corkill RG, et al. Abnormal cerebral blood volume in regions of contused and normal appearing brain following traumatic brain injury using perfusion magnetic resonance imaging. J Neurotrauma. 2001; 18(6):585–593. [PubMed: 11437081]

159. Ge Y, Patel MB, Chen Q, et al. Assessment of thalamic perfusion in patients with mild traumatic brain injury by true FISP arterial spin labelling MR imaging at 3T. Brain injury : [BI]. 2009; 23(7):666–674.

160. Grossman EJ, Jensen JH, Babb JS, et al. Cognitive impairment in mild traumatic brain injury: a longitudinal diffusional kurtosis and perfusion imaging study. AJNR American journal of neuroradiology. 2013; 34(5):951–957. S951–953. [PubMed: 23179649]

161. Lin AP, Liao HJ, Merugumala SK, et al. Metabolic imaging of mild traumatic brain injury. Brain imaging and behavior. 2012; 6(2):208–223. [PubMed: 22684770]

162. Shutter L, Tong KA, Holshouser BA. Proton MRS in acute traumatic brain injury: role for glutamate/glutamine and choline for outcome prediction. J Neurotrauma. 2004; 21(12):1693–1705. [PubMed: 15684761]

163. Henry LC, Tremblay S, Leclerc S, et al. Metabolic changes in concussed American football players during the acute and chronic post-injury phases. BMC neurology. 2011; 11:105. [PubMed: 21861906]

164. Vagnozzi R, Signoretti S, Cristofori L, et al. Assessment of metabolic brain damage and recovery following mild traumatic brain injury: a multicentre, proton magnetic resonance spectroscopic study in concussed patients. Brain. 2010; 133(11):3232–3242. [PubMed: 20736189]

165. Signoretti S, Marmarou A, Fatouros P, et al. Application of chemical shift imaging for measurement of NAA in head injured patients. Acta neurochirurgica Supplement. 2002; 81:373–375. [PubMed: 12168350]

166. Brooks WM, Stidley CA, Petropoulos H, et al. Metabolic and cognitive response to human traumatic brain injury: a quantitative proton magnetic resonance study. J Neurotrauma. 2000; 17(8):629–640. [PubMed: 10972240]

167. Garnett MR, Corkill RG, Blamire AM, et al. Altered cellular metabolism following traumatic brain injury: a magnetic resonance spectroscopy study. J Neurotrauma. 2001; 18(3):231–240. [PubMed: 11284544]

168. Cecil KM, Hills EC, Sandel ME, et al. Proton magnetic resonance spectroscopy for detection of axonal injury in the splenium of the corpus callosum of brain-injured patients. Journal of neurosurgery. 1998; 88(5):795–801. [PubMed: 9576245]

169. Ashwal S, Holshouser B, Tong K, et al. Proton spectroscopy detected myoinositol in children with traumatic brain injury. Pediatric research. 2004; 56(4):630–638. [PubMed: 15295080]

170. Ross BD, Bluml S, Cowan R, et al. In vivo MR spectroscopy of human dementia. Neuroimaging clinics of North America. 1998; 8(4):809–822. [PubMed: 9769343]

171. Babikian T, Freier MC, Ashwal S, et al. MR spectroscopy: predicting long-term neuropsychological outcome following pediatric TBI. Journal of magnetic resonance imaging : JMRI. 2006; 24(4):801–811. [PubMed: 16941608]

172. Brenner T, Freier MC, Holshouser BA, et al. Predicting neuropsychologic outcome after traumatic brain injury in children. Pediatric Neurology. 2003; 28(2):104–114. [PubMed: 12699860]

173. George EO, Roys S, Sours C, et al. Longitudinal and prognostic evaluation of mild traumatic brain injury: A 1H-magnetic resonance spectroscopy study. J Neurotrauma. 2014; 31(11):1018–1028. [PubMed: 24467391]

174. Byrnes KR, Wilson CM, Brabazon F, et al. FDG-PET imaging in mild traumatic brain injury: a critical review. Frontiers in Neuroenergetics. 2013; 5:13. [PubMed: 24409143]

175. Hong YT, Veenith T, Dewar D, et al. Amyloid imaging with carbon 11-labeled Pittsburgh compound B for traumatic brain injury. JAMA neurology. 2014; 71(1):23–31. [PubMed: 24217171]

176. Small GW, Kepe V, Siddarth P, et al. PET scanning of brain tau in retired national football league players: preliminary findings. The American journal of geriatric psychiatry : official journal of the American Association for Geriatric Psychiatry. 2013; 21(2):138–144. [PubMed: 23343487]

177. W G Bradley J. MR appearance of hemorrhage in the brain. Radiology. 1993; 189(1):15–26. [PubMed: 8372185]

KEY POINTS

- Multi-detector CT remains the preferred first line imaging study for moderate and severe traumatic brain injury as it can quickly identify patients who require urgent neurosurgical intervention.
- MRI is significantly more sensitive than CT for detection of pathoanatomic lesions in mild TBI.
- MRI is more sensitive than CT for many types of traumatic injuries and plays a complementary role. It is most indicated in the acute setting for mild TBI when a patient's symptoms and/or neurologic exam are not explained by CT findings.
- Emerging advanced neuroimaging techniques may improve the sensitivity for identifying mild TBI as well as offer prognostic information for all grades of injury.

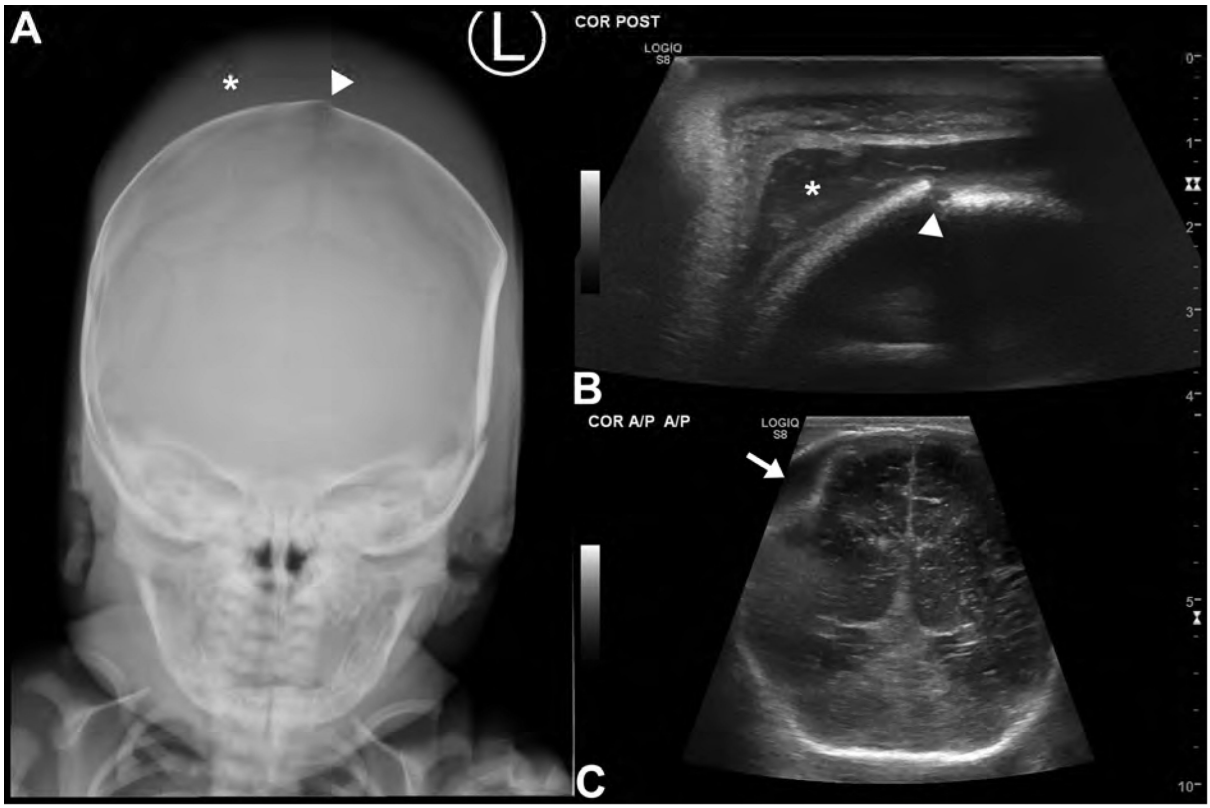

Figure 1. Evaluation of neonatal traumatic brain injury with ultrasound and radiographs

AP skull radiograph (**A**) and coronal ultrasound images (**B,C**) in a newborn reveal a traumatic injury suffered during a difficult forceps delivery. Skull radiograph (**A**) reveals a fracture of the parietal calvarium (arrowhead) as well as scalp soft tissue swelling compatible with a subgaleal hematoma (asterisk). High frequency (10 MHz) ultrasound of the scalp (**B**) with a linear transducer shows the extracranial subgaleal hematoma in better detail (asterisk) and again demonstrates the fracture (arrowhead). By positioning a lower frequency (6 MHz) vector transducer over a fontanel, images of the brain parenchyma and superior extra-axial spaces are obtained (**C**). These reveal a biconvex extra-axial collection (arrow) along the right parietal convexity, consistent with an epidural hematoma. While ultrasound and radiographs generally do not play a role in the evaluation of TBI, they can be useful for problem solving in limited pediatric imaging scenarios.

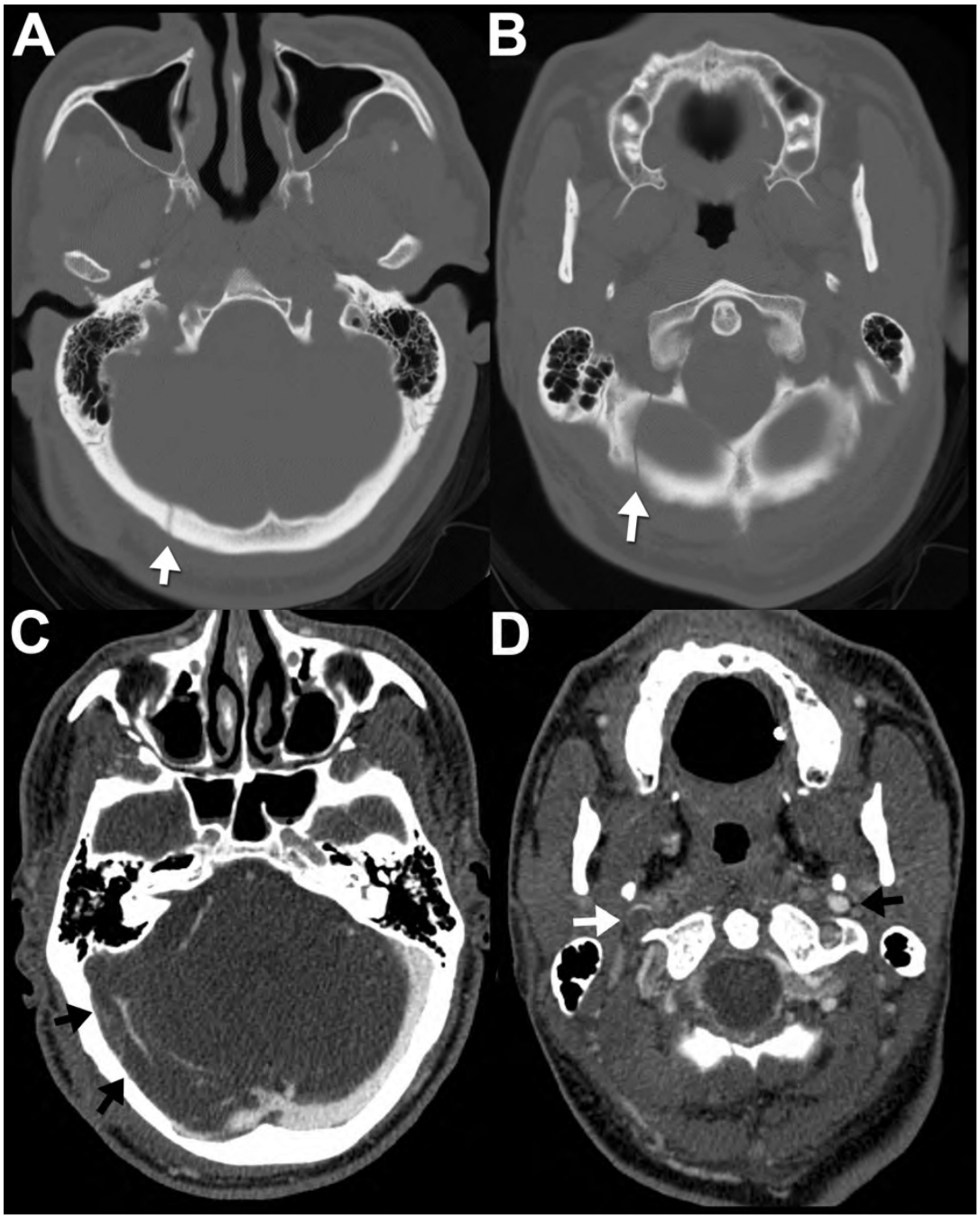

Figure 2. Occipital fracture complicated by transverse sinus injury

42-year-old man presents after fall with impact to the back of the head. Noncontrast head CT viewed at bone window technique (**A,B**) reveals a nondisplaced, linear right occipital fracture (arrows) adjacent to the expected location of the right transverse sinus. Therefore, a CT venogram was subsequently performed to evaluate for venous sinus injury. Note the thrombus, manifested as unopacified flow within the right transverse sinus (**C**, arrows) that extends into the right sigmoid sinus and the right jugular vein (**D**, white arrow.) The normal left jugular vein (**D**, black arrow) is shown for comparison.

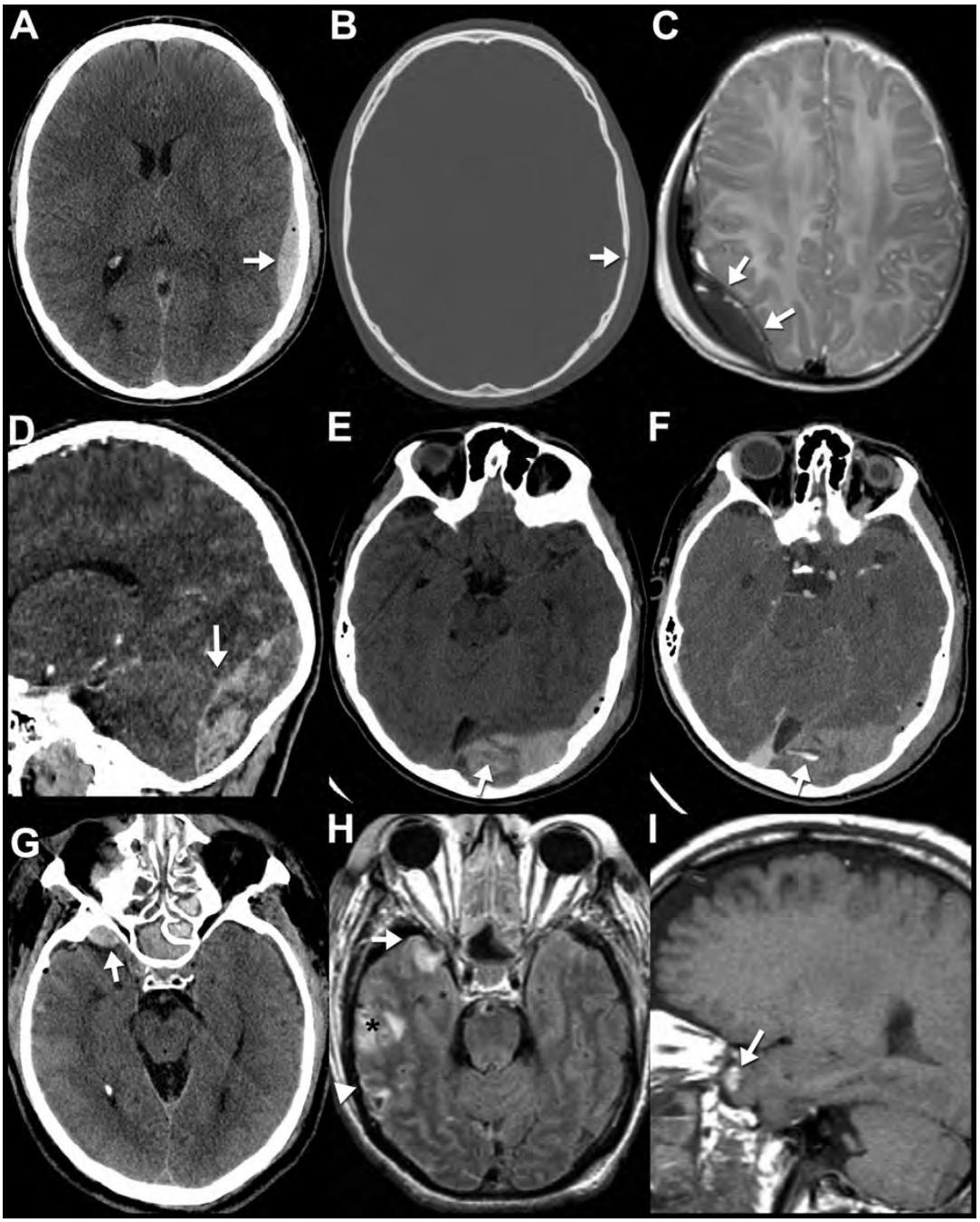

Figure 3. CT and MR appearance of epidural hematoma

Noncontrast CT (**A,B**) performed on a 26-year-old man who was “found down” with altered mental status. Note the classic biconvex hyperdense epidural hematoma with an overlying nondisplaced calvarial fracture (arrows). Axial T2WI (**C**) from a “rapid” MR protocol in a different patient (3-month-old accidentally dropped on her head) reveals a right parietal biconvex low signal epidural collection. Note the position of the dura, seen as the thin black line deep to the collection (arrows); this allows confident determination that the collection is located in the epidural space. Sagittal (**D**) and axial (**E**) reformatted images from a

noncontrast CT performed in a different patient (13-year-old male after a skateboard accident) show a heterogeneous epidural hematoma in the occipital region. Areas of lower density within the hematoma likely represent hyperacute unclotted blood concerning for active bleeding and predictive of continued expansion of the hematoma. This is confirmed on the CTA of the head performed minutes later (**F**) where dense contrast material extravasates (**F**, arrow) into the area of low density on the earlier noncontrast study (**E**, arrow). The sagittal reformatted images (**D**) best demonstrate how the hematoma crosses the plane of the tentorium cerebelli (arrow) into the posterior fossa, characteristic of epidural hematomas (unlike subdural hematomas) as they are not constrained by dural boundaries. In contrast to arterial epidural hematomas, venous epidural hematomas bleed under lower pressure and are therefore less likely to increase in size. Noncontrast CT (**G**), axial FLAIR (**H**) and sagittal T1WI (**I**) performed on a 52-year-old victim of assault reveal a right sphenoparietal venous epidural hematoma (arrows). CT on the day of the injury (**G**) shows the characteristic well-defined, crescentic, high-density extra-axial collection (white arrow) along the anterior margin of the middle cranial fossa. On MRI performed 2 days later (**H,I**), the same venous epidural hematoma (arrow) appears isointense to adjacent anterior temporal contusion on FLAIR (**H**) and hyperintenseT1WI (**I**), consistent with intracellular methemoglobin blood products and it has not increased in size. In cases of trauma, multiple pathologic entities often are seen in the same examination. Notably, foci of subarachnoid hemorrhage (white arrowhead) and temporal lobe contusions (black asterisk) are much more visible on MRI (**H**) than CT.

In contrast to arterial epidural hematomas, venous epidural hematomas bleed under lower pressures and are less likely to expand. Noncontrast CT (**G**), axial FLAIR (**H**) and sagittal T1WI (**I**) performed on a 52-year-old victim of assault reveal a right sphenoparietal venous epidural hematoma (arrows). CT on the day of the injury (**G**) shows a characteristic lobular high-density extra-axial collection (white arrow) along the anterior margin of the middle cranial fossa. On MRI performed 2 days later (**H,I**), the same venous epidural hematoma is seen adjacent to an anterior temporal contusion (**H** (**I**). In cases of trauma, multiple pathologic entities often are seen in the same examination. Notably, linear foci of subarachnoid hemorrhage (white arrowhead) and temporal lobe contusion (asterisk) are much more visible on MRI (**H**) than CT (**G**).

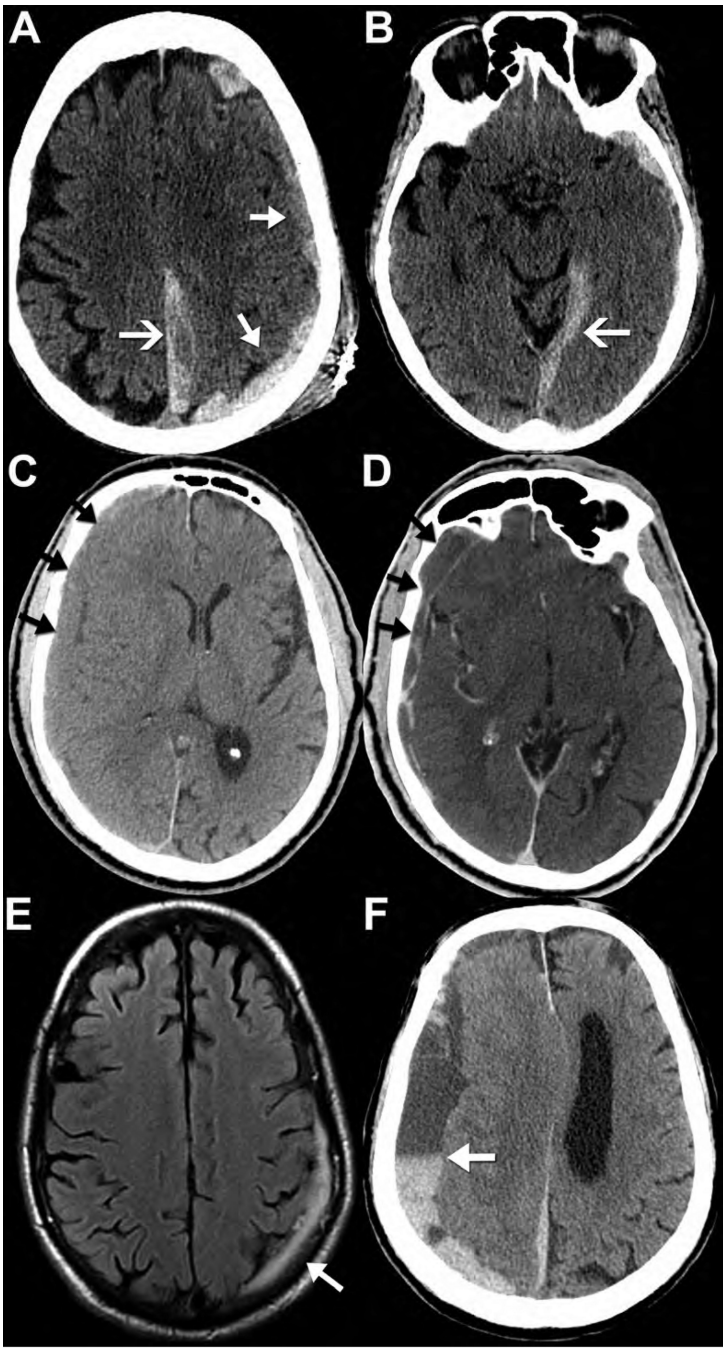

Figure 4. CT and MR appearance of subdural hematomas

Noncontrast CT (**A,B**) performed on a 90-year-old female after fall with left parietal scalp laceration reveals hyperdense blood along the left convexity (**A**, closed arrows), left posterior falx cerebri (**A**, open arrow), and tentorium cerebelli (**B**, open arrow). Note how the subdural hematomas do not cross the dural sinuses to the other side of the falx or tentorium. Noncontrast CT performed on an 82-year-old man after falling shows a right convexity subacute subdural hematoma that is isodense to the adjacent cortex (**C**, arrows). Post-contrast imaging is generally not required for evaluation of a subdural hematoma;

however, it was obtained in this case. The post-contrast CT (**D**, arrows) images demonstrate peripheral enhancement of the collection without evidence of active extravasation, thus reinforcing a subacute injury. Axial FLAIR MR image (**E**) from a 69-year-old man after head trauma exemplifies the high contrast difference on MR between the FLAIR hyperintense subdural hematoma (arrow) and the adjacent hypointense calvarium. Axial noncontrast CT (**F**) from a different patient, a 73-year-old man with left-sided weakness, shows the appearance of a mixed-density, “acute-on-chronic” subdural hematoma along the right convexity and falx cerebri. Note the dependent layering of the acute, denser blood products within the chronic, hypodense collection; this is often referred to as the “hematocrit sign” (arrow).

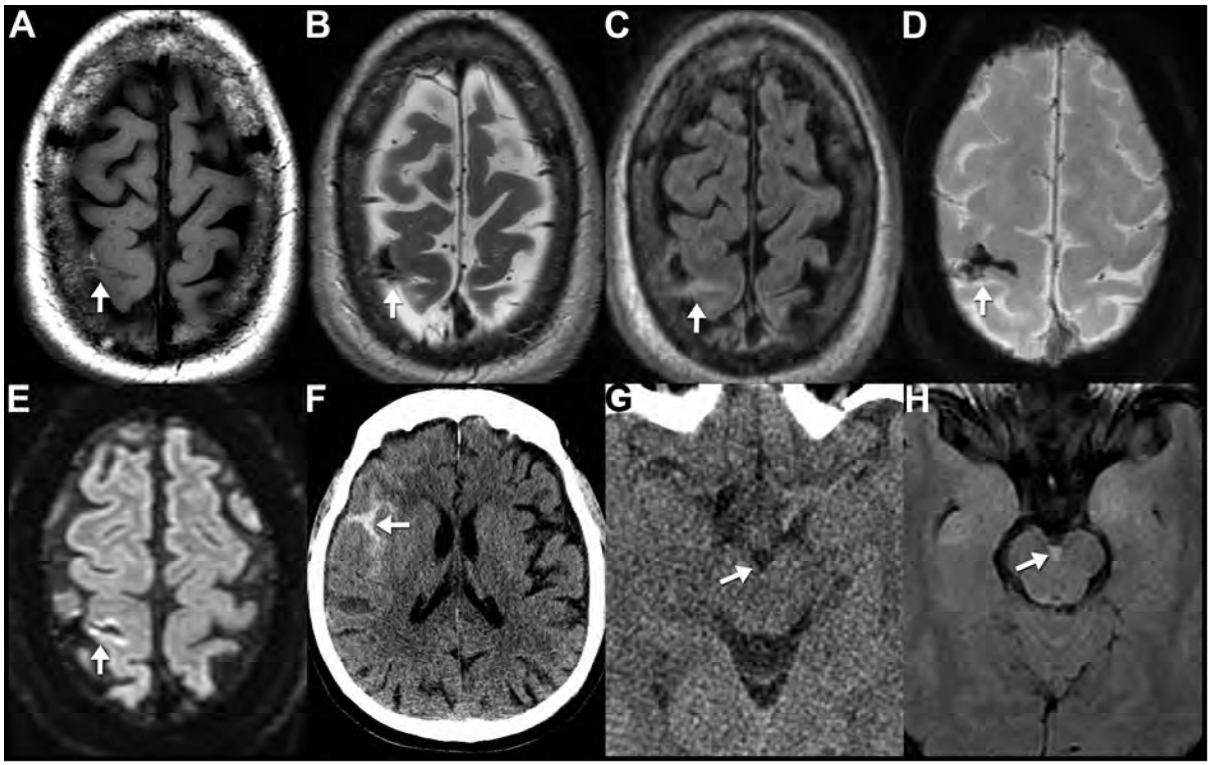

Figure 5. CT and MR appearance of subarachnoid hemorrhage

MRI (**A-E**) performed on a 58-year-old man who presented 3 days after a fall with altered mental status. Subacute subarachnoid hemorrhage appears hyperintense to brain on T1WI (**A**) and hypointense on T2WI (**B**). Subarachnoid hemorrhage does not suppress like normal CSF on FLAIR imaging (**C**) and it appears markedly hypointense on SWI (**D**). The linear area of reduced diffusion in the cortex adjacent to the subarachnoid hemorrhage likely represents adjacent cerebral contusion (**E**). This is a good example showing the appearance of early subacute subarachnoid blood products within the central sulcus on multiple pulse sequences (arrows). Noncontrast CT (**F**) from a 70-year-old male after syncope and fall with head injury shows the classic appearance of acute subarachnoid hemorrhage in the right sylvian fissure (arrow). Noncontrast CT (**G**) and FLAIR (**H**) images obtained the same day in a 33-year-old female after a motor vehicle crash. The trace interpeduncular subarachnoid hemorrhage (arrow) is invisible on CT (**G**), but is readily apparent on MR (**H**), highlighting the greater sensitivity of MR to blood products.

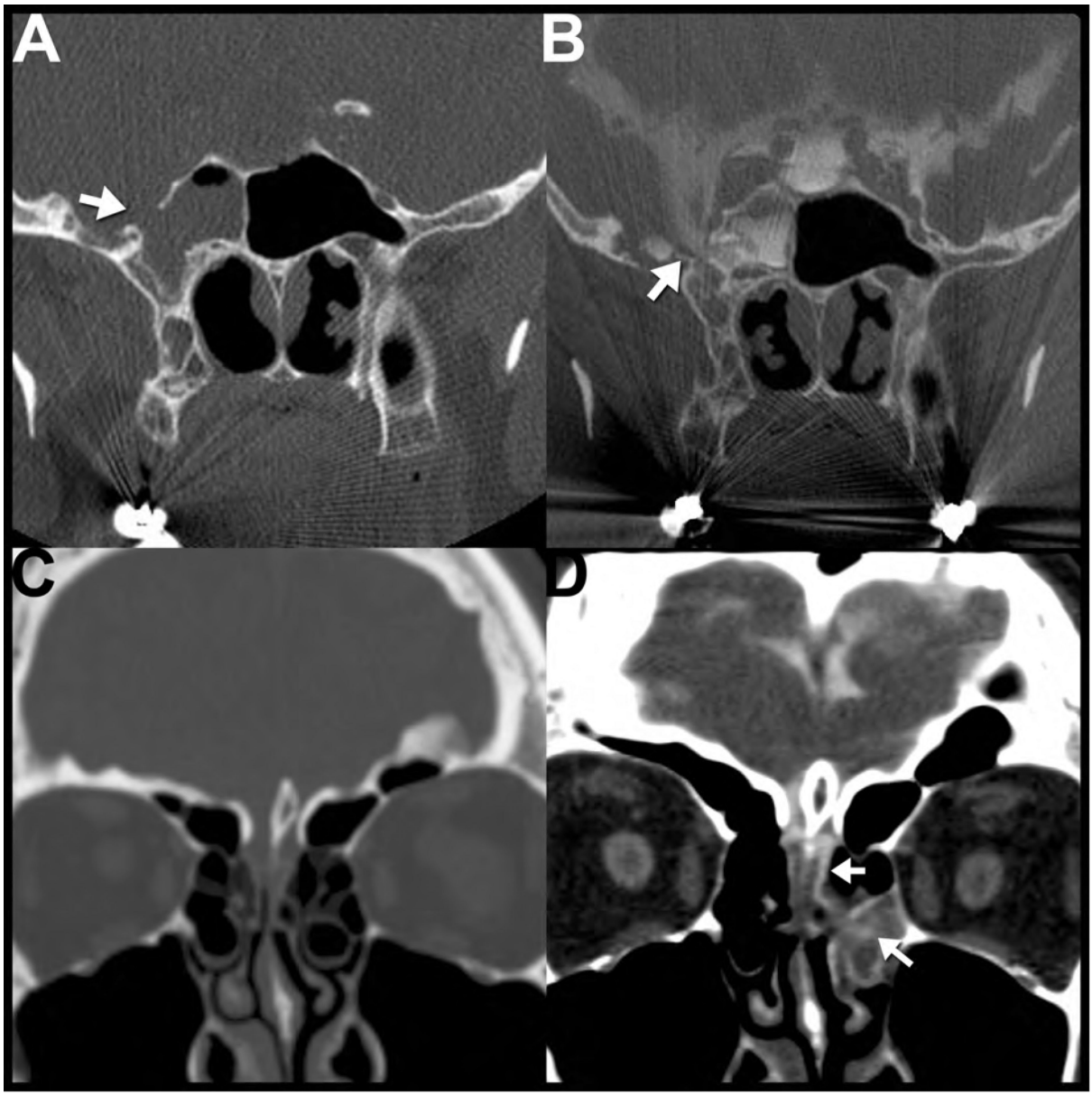

Figure 6. Imaging evaluation of patients with CSF leaks

Coronal reformatted images from a noncontrast CT (**A,C**) and CT cisternograms (**B,D**) performed in 2 different patients with posttraumatic CSF leaks. The first patient (**A,B**) is a 55-year-old female with a history of remote trauma and meningitis. Note the opacified right sphenoid sinus with a large bony defect between the lateral wall of the right sphenoid sinus and the middle cranial fossa (**A**, arrow). CT cisternography was performed (**B**), confirming abnormal leakage of CSF contrast from the middle cranial fossa into the sphenoid sinus. The second patient (**C,D**) is a 33-year-old female with CSF rhinorrhea (confirmed with positive B_2-Transferrin test) after facial trauma. Noncontrast CT (**C**) reveals subtle unilateral opacification of the left olfactory recess concerning for a possible cephalocele, but it did not show a definitive bony abnormality in that region. The patient returned two weeks later and

a CT cisternogram was performed (**D**) revealing abnormal passage of CSF contrast (arrows) through the left cribiform plate through the left olfactory recess and into the nasal cavity.

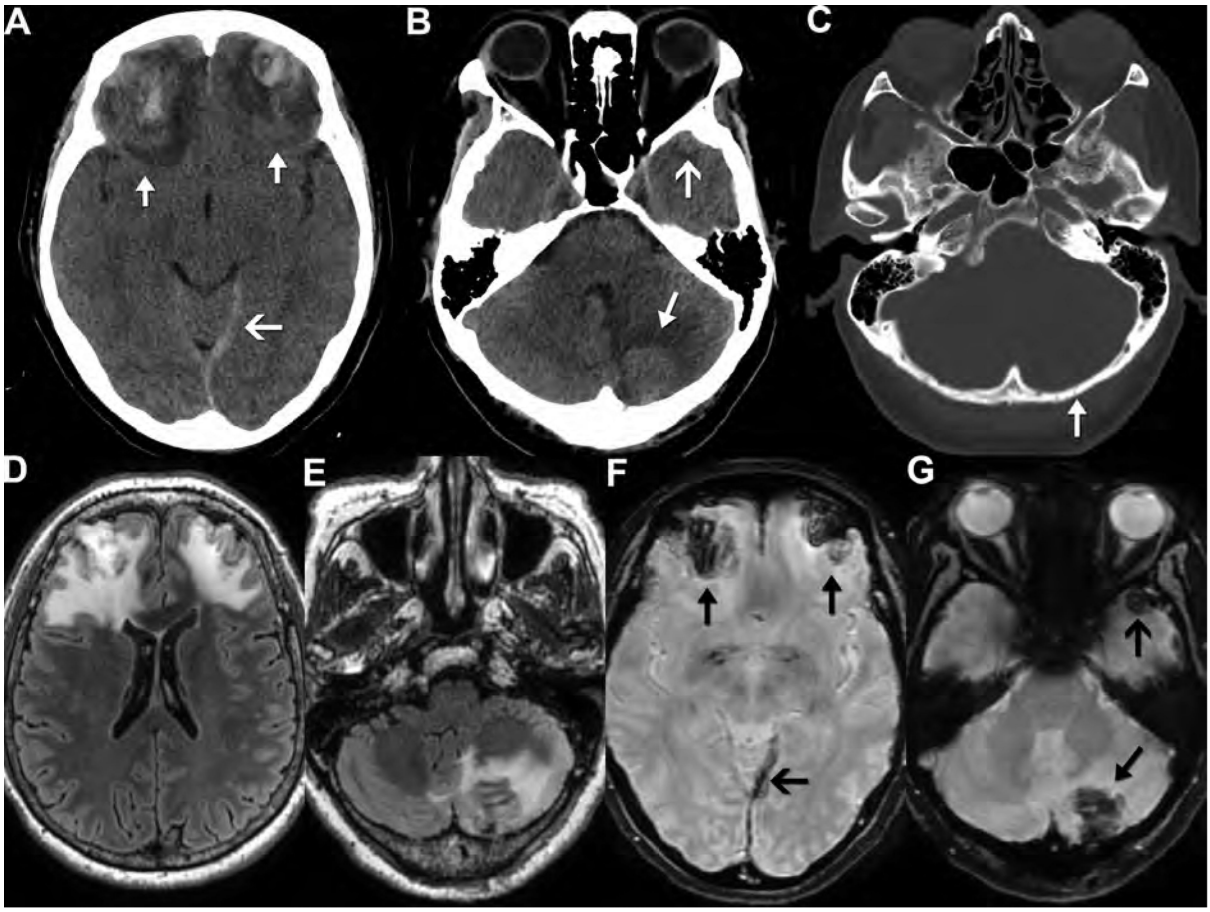

Figure 7. CT and MR appearance of cerebral and cerebellar contusion

Noncontrast CT (**A-C**) and FLAIR and susceptibility-weighted MR (**D-G**) images obtained on a 59-year-old woman after a fall that occurred 5 days earlier. CT images show a nondisplaced left occipital fracture (**C**, arrow) with an underlying hemorrhagic contusion in the left cerebellar hemisphere (**B**, closed arrow) compatible with coup injury. There are also large, bifrontal, hemorrhagic contusions (**A**, closed arrows) and a small left anterior temporal hemorrhagic contusion (**B**, open arrow), compatible with contrecoup injuries. These lesions have a predictable appearance on MR with low signal on SWI (**F**, closed arrows; **G**, arrows) and a large area of surrounding edema on FLAIR images (**D,E**). Also note the increased prominence of the left tentorial subdural hematoma (open arrow) on MR SWI (**F**) compared to CT (**A**).

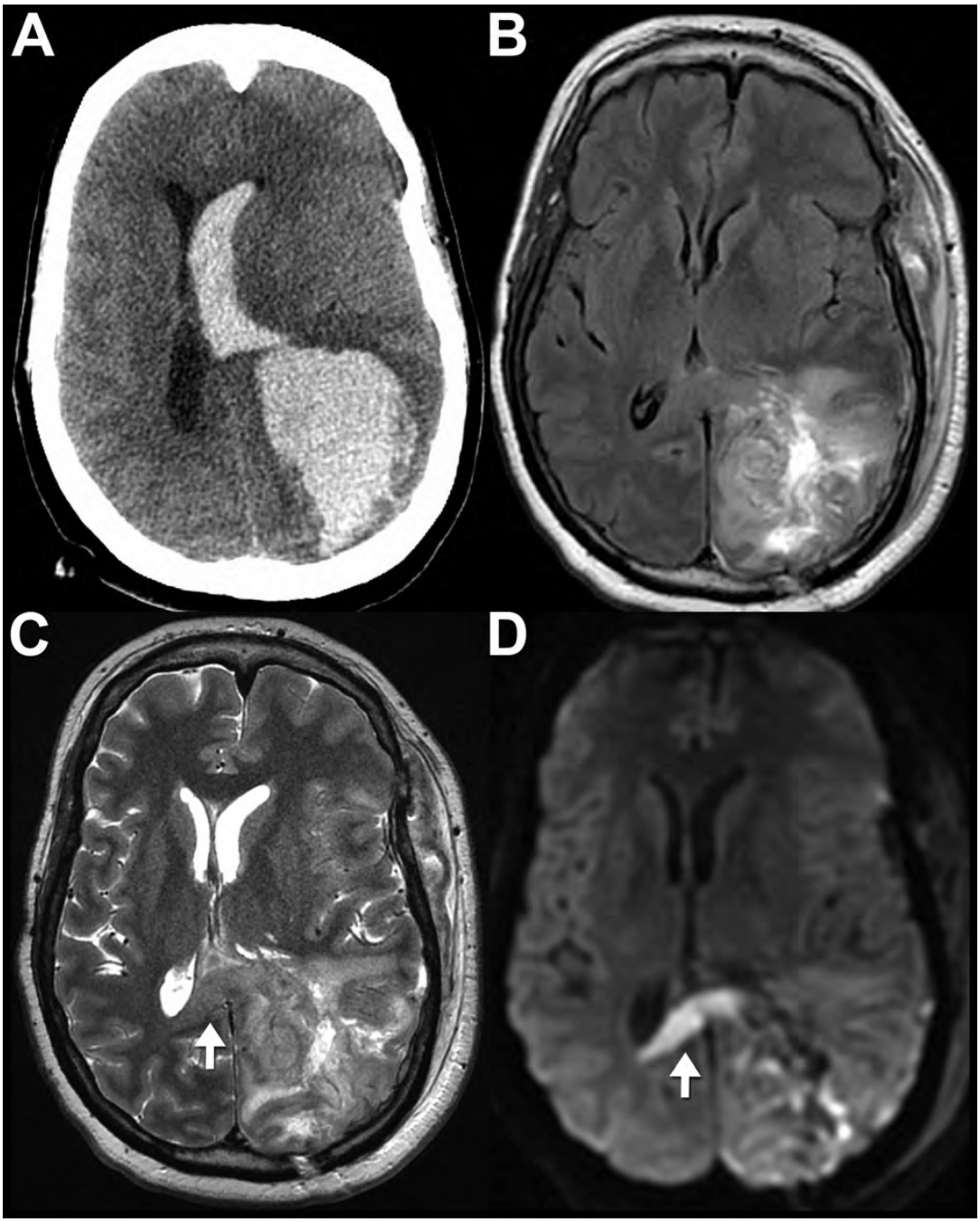

Figure 8. CT and MR appearance of intracerebral hematoma

Noncontrast CT (**A**) of 61-year-old male after head trauma reveals a large, hyperdense, acute left parietal hematoma with surrounding edema that has decompressed into the adjacent left lateral ventricle (intraventricular hemorrhage). MRI performed 11 days later (**B-D**) shows decreased edema with residual T2 hyperintense blood products (likely corresponding to “late subacute” extracellular methemoglobin). Increased T2 signal intensity (**C**) and reduced diffusion (**D**) in the splenium of the corpus callosum (arrows) is likely a result of Wallerian

degeneration of the axons leading away from the left parietal injury, and not traumatic axonal injury of the splenium.

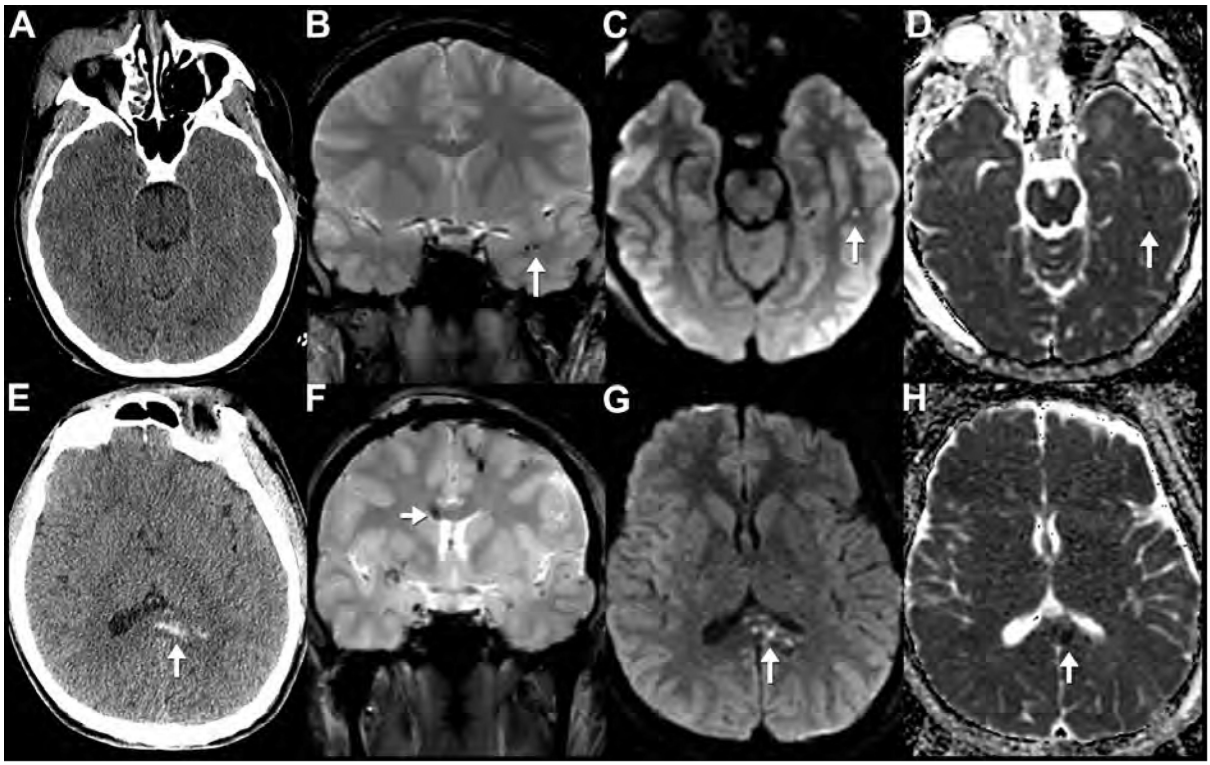

Figure 9. CT and MR appearance of traumatic axonal injury

Initial noncontrast CT (**A**) of a 24-year-old female after a helmeted bicycle accident with brief loss of consciousness shows right periorbital soft tissue swelling, but is otherwise normal. MRI (including T2*-weighted MPGR (**B**), DWI (**C**) and ADC map (**D**) obtained the following day shows scattered foci of reduced diffusion and increased susceptibility, compatible with traumatic axonal injuries. Example lesions include a focus of reduced diffusion (**C**, arrow) with low ADC value (**D**, arrow) and foci of increased susceptibility (**B**, arrow) in the left temporal stem subcortical white matter. A different patient presented after an assault (**E-H**). This patient's noncontrast CT shows multiple areas of hemorrhagic axonal shearing injury involving the splenium of the corpus callosum (**E**, arrow). This area shows reduced diffusion (**G**, arrow), low ADC value (**H**, arrow) and increased susceptibility on MPGR (**F**, arrow) on MRI performed the same day. The coronal MPGR image (**F**) also reveals numerous additional white matter shear injuries (low signal) compatible with diffuse axonal injury.

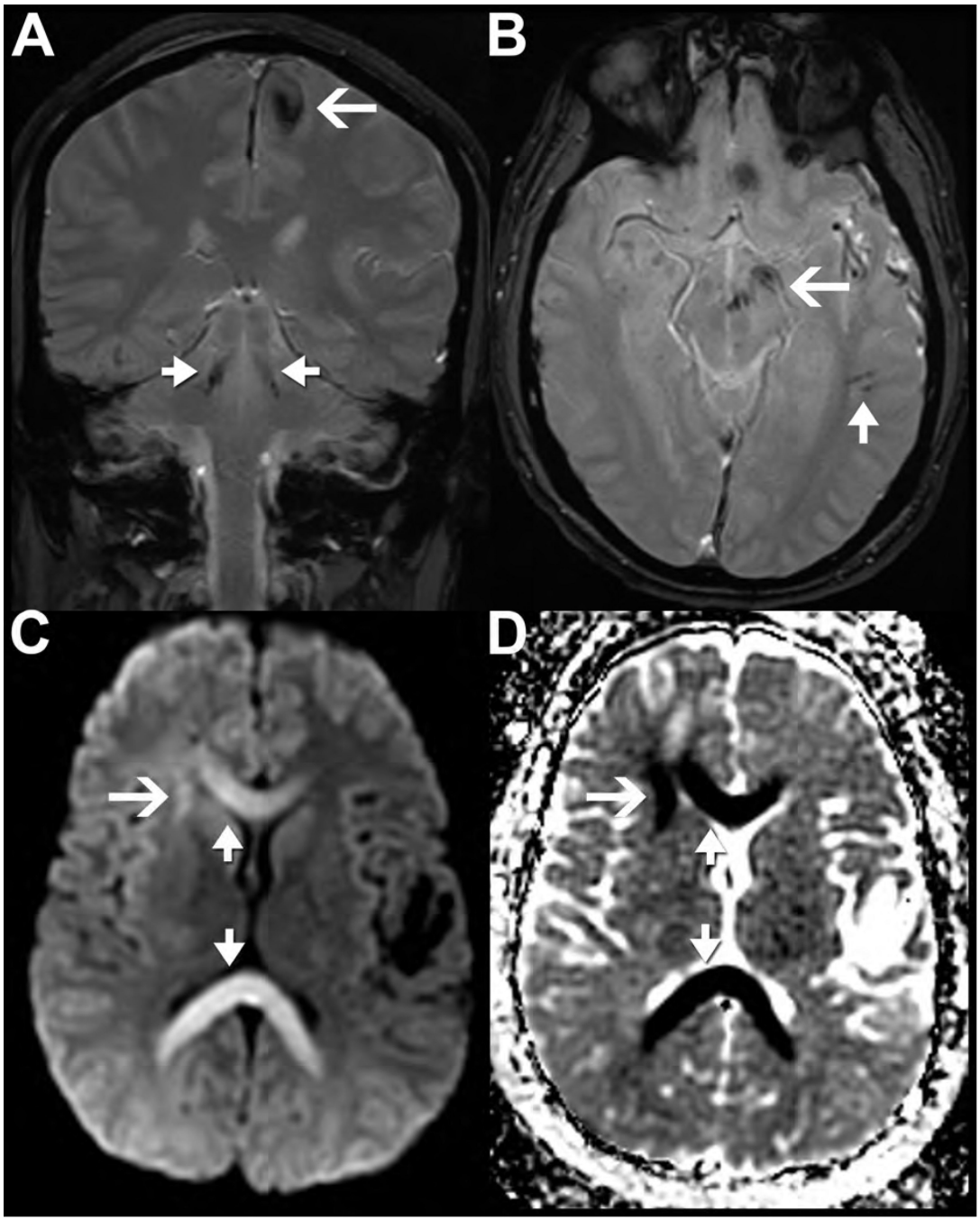

Figure 10. MR appearance of Grade 3 diffuse axonal injury

MPGR (**A,B**), DWI (**C**), and ADC map MR images of a 23-year-old man with head trauma after a motorcycle accident. MPGR images reveal foci of susceptibility in the subcortical white matter of the parietal (open arrow, **A**) and temporal lobes (closed arrow, **B**) as well as infratentorial injury to the bilateral superior cerebellar peduncles (closed arrows, **A**) and midbrain and cerebral peduncle (open arrow, **B**) secondary to traumatic axonal injury. There are also extra-axial foci of susceptibility along the falx compatible with a subdural hematoma (**A,B**). DWI (**C**) and ADC map (**D**) from the same patient reveal marked reduced

diffusion in the genu and splenium (closed arrows) of the corpus callosum also consistent with a combination of Wallerian and axonal injury. Note how the entire right frontal lobe white matter shows abnormal reduced diffusion (open arrow in **C,D**), with a more focal insult to the anterior subinsular region.

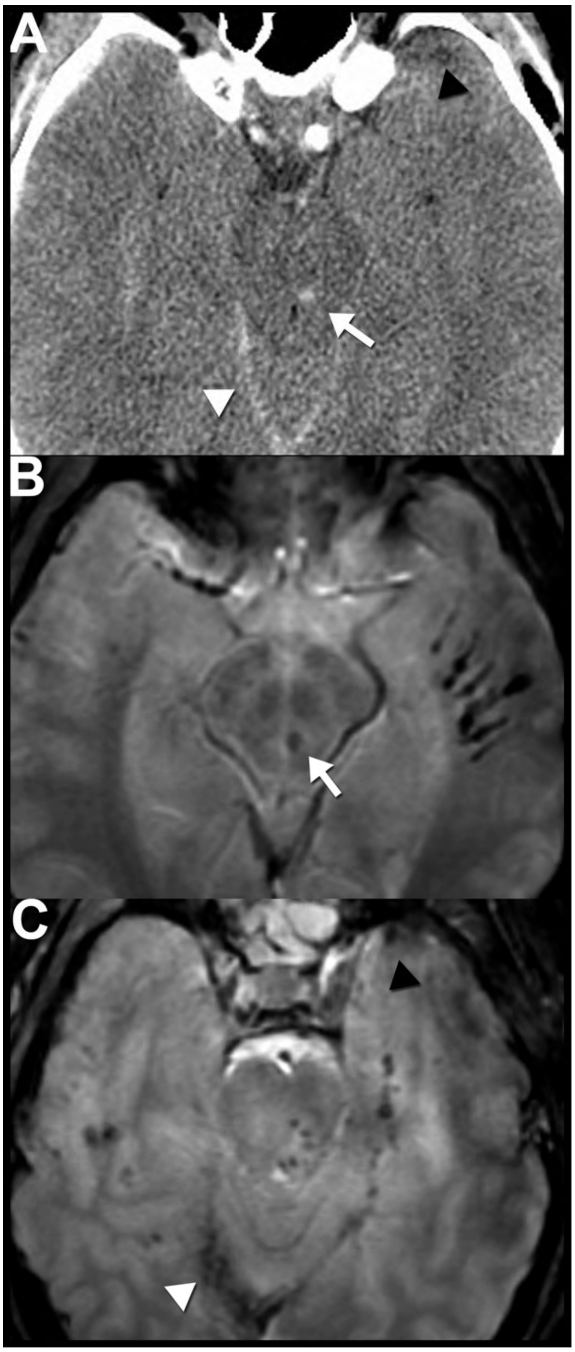

Figure 11. CT and MR appearance of brainstem injury with diffuse axonal injury

Axial noncontrast CT (**A**) and T2*-weighted MPGR MR (**B,C**) images of 27-year-old man reveal posttraumatic brainstem injury. Hemorrhagic axonal injury in the midbrain tegmentum appears as rounded hyperdensity on CT (**A**, arrow) and as a focal area of susceptibility on MPGR sequence (**B**, arrow). Caudally, an axial MPGR image through the pons (**C**) reveals multiple additional foci of susceptibility in the dorsal pons that were not apparent on CT. Numerous additional foci of abnormal susceptibility (**B,C**) are present in the bilateral temporal supratentorial and infratentorial white matter consistent with diffuse

axonal injury. Also note traumatic injuries including a right tentorial subdural hematoma (white arrowheads) and a left anterior temporal contusion (black arrowheads), which are better appreciated on MR (**C**) than CT (**A**).

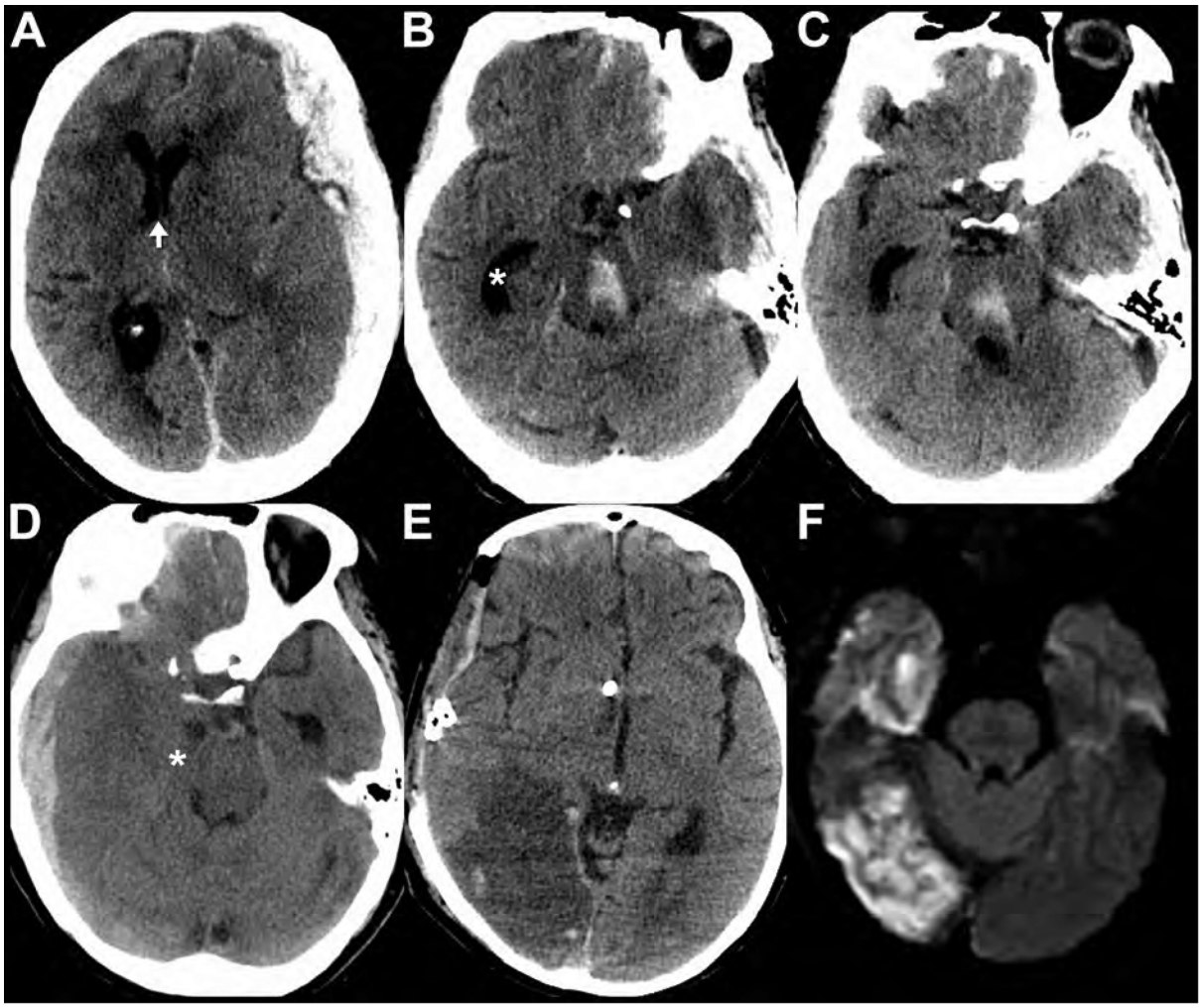

Figure 12. Secondary traumatic brain injuries in patients with TBI

Axial noncontrast CT images (**A-C**) from an 80-year-old female reveal left convexity holohemispheric and parafalcine subdural hematomas. Secondary complications resulting from mass effect from the hematomas include left to right midline shift (arrow shows position of the septum pelucidum) with subfalcine herniation (**A**), left uncal and downward transtentorial herniation (**B,C**), trapping of the temporal horn (asterisk) of the right lateral ventricle secondary to obstruction of the foramen of Monro (**B,C**), and a Duret hemorrhage in the midbrain (**B**) and pons (**C**). Images from a different patient show secondary complications in a 74-year-old female after TBI. The preoperative noncontrast CT (**D**) images demonstrate mass effect from a right holohemispheric subdural hematoma resulting in right uncal herniation and trapping of the temporal horn of the left lateral ventricle. The right temporal horn is nearly midline in location (asterisk. The post-operative noncontrast CT obtained later that evening (**E**) reveals a decompressive craniectomy, ventricular drain placement, and a new large hypodensity involving the territory of the right posterior cerebral artery (PCA) vascular territory, consistent with infarction. Diffusion weighted MRI (**F**) obtained 4 days after initial injury confirms the right PCA territory infarct, secondary to compression of the proximal PCA by the previously herniated right uncus.

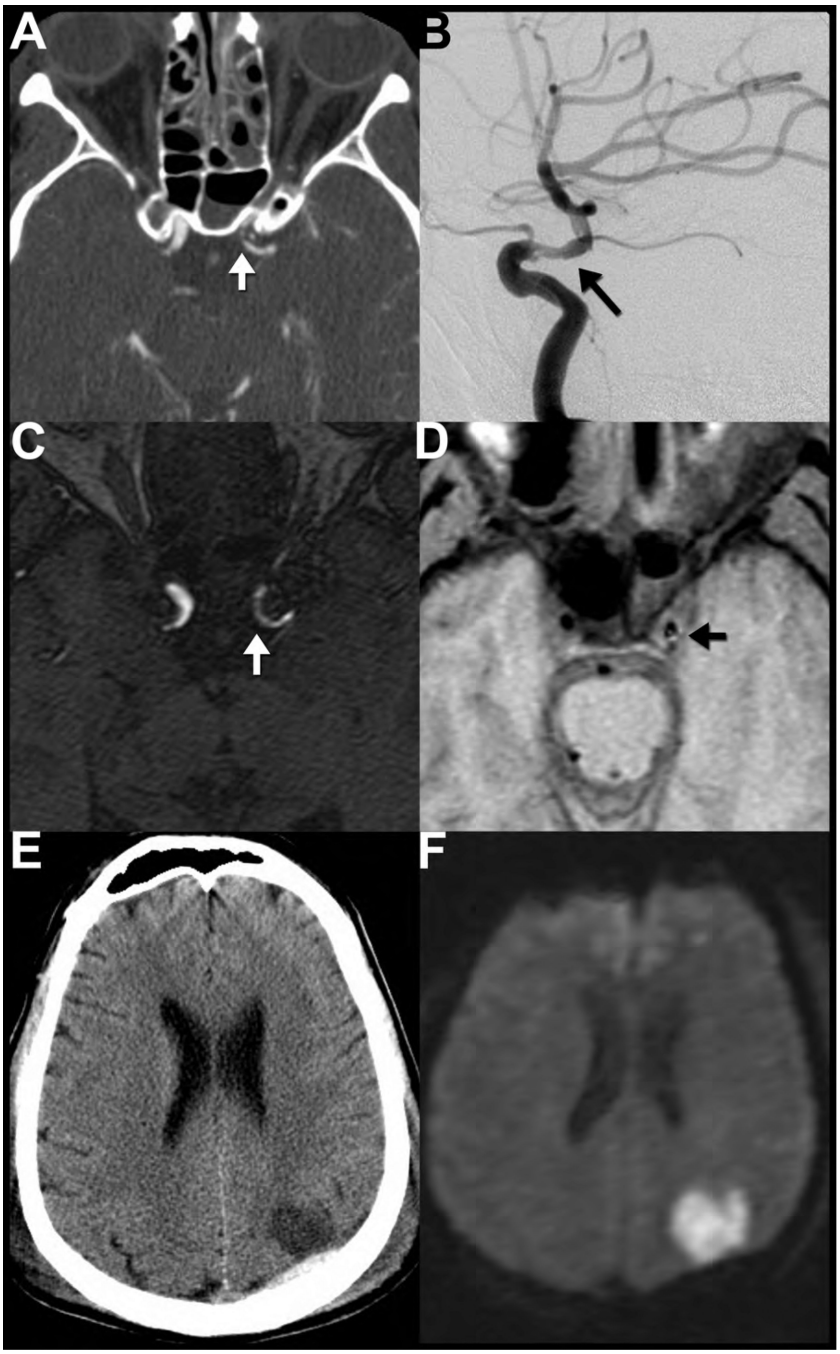

Figure 13. Traumatic vascular dissection of the supraclinoid internal carotid artery

CTA (**A**) performed the day after injury shows asymmetric narrowing and luminal irregularity of the left internal carotid artery (ICA) (arrow) just beyond the anterior clinoid process concerning for traumatic dissection. Note the air-hemorrhage level within the left sphenoid sinus (**A**) which should raise suspicion anterior skull base fracture (not shown) and potential injury to the adjacent carotid artery. Dissection of the left supraclinoid ICA was confirmed the same day on digital subtraction angiography (**B**), which again revealed an irregular, narrowed lumen (arrow). Time of flight MR angiogram (**C**) performed 3 days after

injury shows a narrowed irregular lumen of the left supraclinoid ICA (arrow). T1WI (**D**) from the same examination reveals subtle T1-shortening (arrow) in the left ICA wall, consistent with early subacute methemoglobin blood products within a dissecting intramural hematoma. Noncontrast CT (**E**) and diffusion weighted MRI (**F**) obtained 2 and 3 days after injury, respectively, show that the patient's dissection was complicated by an acute left middle cerebral artery territory embolic infarction.

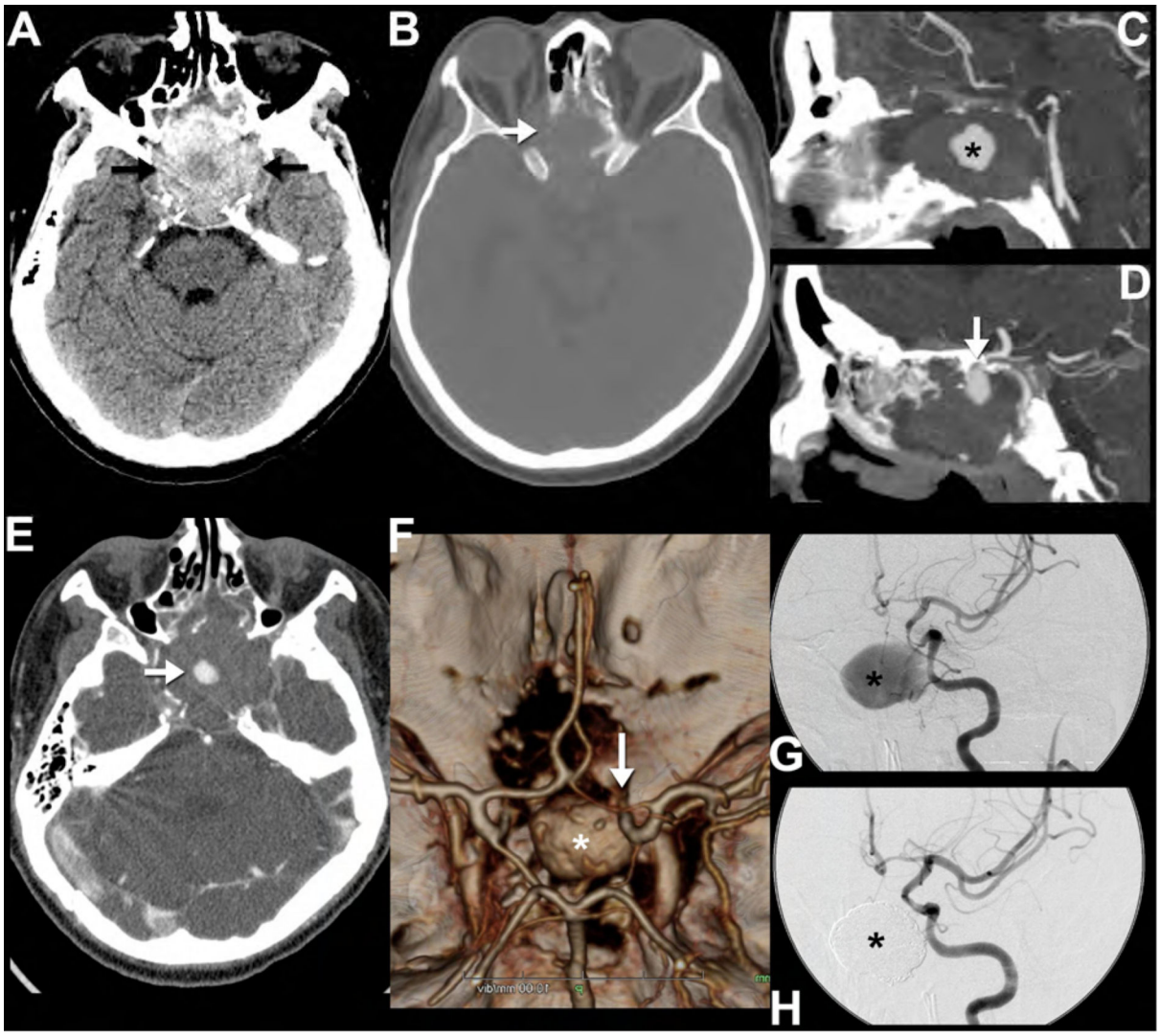

Figure 14. Postraumatic pseudoaneurysm

This 43-year-old man presented with headache and visual symptoms 3 months after suffering facial fractures in a motor vehicle accident. Noncontrast CT reveals a large hyperdense mass (arrows) within the anterior skull base (**A**) eroding the sphenoid bone, sella and the orbits (arrow) (**B**). Sagittal reformatted CT angiography images performed the same day show the central area of the mass enhancing (asterisk) to the same extent as the adjacent intracranial arteries (**C**). In addition, there is an apparent narrow-necked connection (arrow) between the enhancing portion and the left cavernous internal carotid artery (**D**), consistent with a pseudoaneurysm. Note that the central low density (**A**, asterisk) within the higher density, thrombosed portion of the pseudoaneurysm correlates with the central nonthrombosed, enhancing area (**E**, arrow) on the postcontrast images. 3D reformatted images of the circle of Willis (**F**) highlight the relationship of the pseudoaneurysm (asterisk); note that only the nonthrombosed portion is visualized) to the left internal carotid artery (arrow). Catheter angiography images following injection of the left internal carotid

artery show the appearance of the pseudoaneurysm (asterisk) before (**G**) and after (**H**) treatment with endovascular coil embolization.

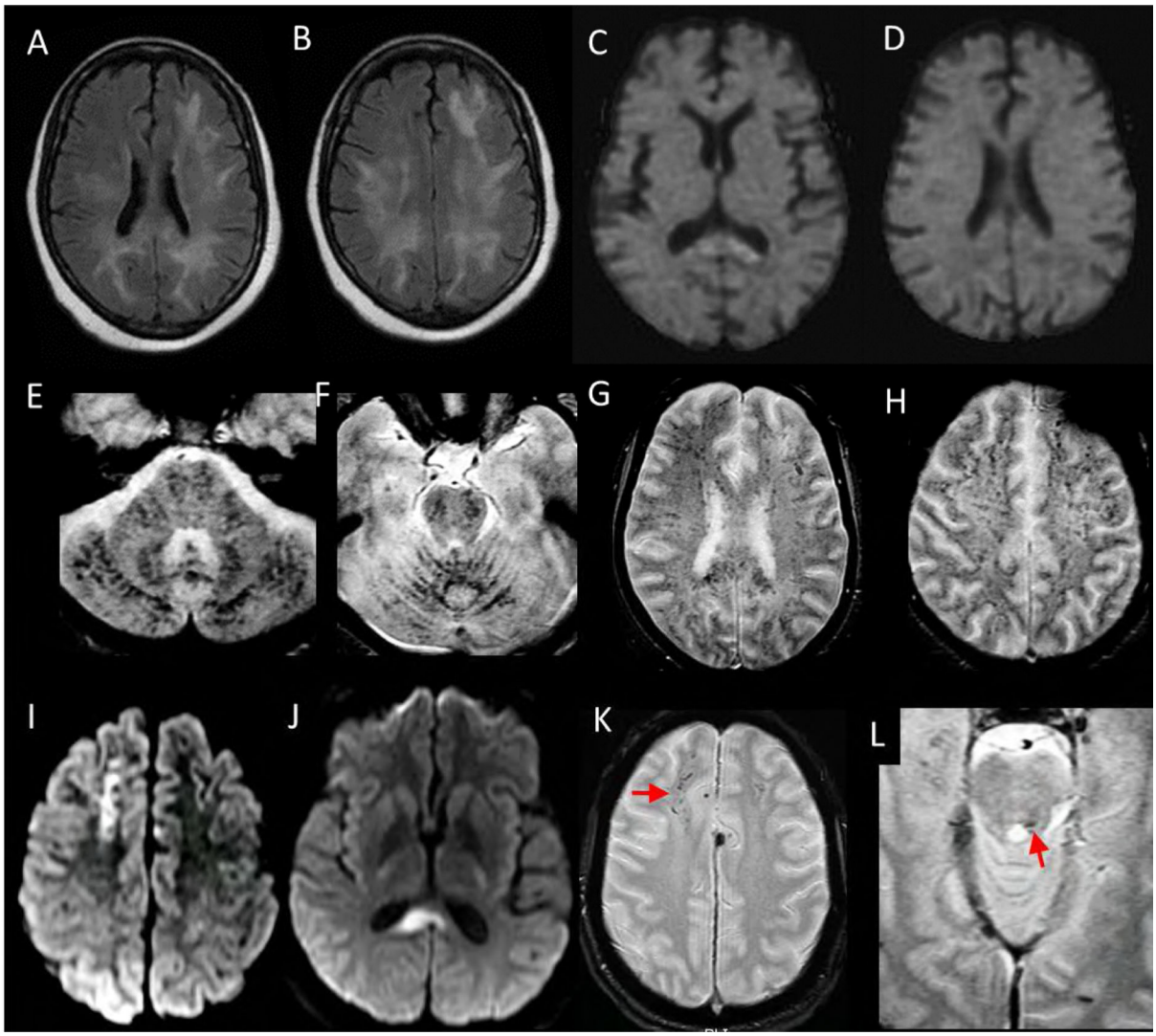

Figure 15. Cerebral Fat Embolism Syndrome (CFES) as a mimic of DAI:

65 year old woman with progressive lethargy and coma in setting of multiple bone infarcts and cerebral fat embolism syndrome confirmed on autopsy. Axial FLAIR (**A, B**) and diffusion (**C, D**) weighted images demonstrate confluent FLAIR hyperintense white matter signal abnormality with relatively little diffusion signal abnormality, which is isolated to the splenium of the corpus callosum. Axial susceptibility-weighted imaging (**E-H**) reveal innumerable foci of susceptibility artifact throughout the infratentorial and supratentorial brain consistent with a pattern of cardio-embolic showering with resultant micro-hemorrhages. In comparison, axial DWI (**I, J**) from a brain MRI performed on a 42 year old man 7 days after a motor vehicle collision shows clustered, confluent foci of reduced diffusion most prominent in the right juxta-cortical frontal lobe and splenium of the corpus callosum related to DAI. T2* weighted gradient echo sequences (**K, L**) reveal asymmetric clustered foci of susceptibility artifact in the right greater than left juxtacortical frontal lobe white matter (arrow in **K**) and dorsal pontomedullary junction near the left superior cerebellar peduncle (arrow in **L**). Compared with CFES, susceptibility artifact secondary to

DAI tends to be more sparse, clustered, and irregular in distribution. In addition, CFES more commonly affects the cerebellum.

Table 1

Glasgow Coma Scale

BEHAVIOR	RESPONSE	SCORE
Eye opening response	Spontaneously	4
	To speech	3
	To pain	2
	No response	1
Best verbal response	Oriented to time, place, and person	5
	Confused	4
	Inappropriate words	3
	incomprehensible sounds	2
	No response	1
Best motor response	Obeys commands	6
	Moves to localized pain	5
	Flexion withdrawal from pain	4
	Abnormal flexion (decorticate)	3
	Abnormal extension (decerebrate)	2
	No response	1
Total score:		___
	Best response	15
	Comatose patient	8 or less
	Totally unresponsive	3

From Teasdale G, Jennett B. Assessment of coma and impaired consciousness. A practical scale. Lancet. 1974 Jul 13;2(7872):81-4; with permission.

Table 2

Recommended MR Protocol for TBI

Field Strength	**1.5T**			**3T**		
	Sequence	**Orientation**	**Imaging time (min)**	**Sequence**	**Orientation**	**Imaging time (min)**
Preferred Sequences	3D T1W	Sagittal	8	3D T1W	Sagittal	4
	T2W FSE	Axial	3	3D T2W	Sagittal	4
	T2W FLAIR	Axial	3	T2W FLAIR	Axial	3
	DWI EPI	Axial	2	DWI EPI	Axial	2
	3D SWI	Axial	8	3D SWI	Axial	6
			Total: 24			**Total:** 19
Alternatives Sequences	T1W SE *	Sagittal	3	T2W FSE †	Axial	3
	2D GRE ‡	Axial	3	2D GRE §	Axial	3

From Haacke EM, Duhaime AC, Gean AD, et al. Common data elements in radiologic imaging of traumatic brain injury. Journal of magnetic resonance imaging : JMRI 2010;32(3):516-543; with permission.

* Option if 3D T1W is not available

† Option if 3D T2W is not available

‡ Option if 3D SWI is not available

Table 3

Appearance of Aging Blood on MR Sequences

	Time frame	Molecular Species	Celluar compartment	T1WI signal[§]	T2WI signal[††]
Hyperacute	<24 h	Oxyhemoglobin	Intracellular	Isointense	Iso-/Hyperintense
Acute	1-3 d	Deoxyhemoglobin	Intracellular	Iso-/Hypointense	Hypointense
Early Subacute	3-7 d	Methemoglobin	Intracellular	Hyperintense	Hypointense
Late Subacute	7-14 d	Methemoglobin	Extracellular	Hyperintense	Hyperintense
Chronic	>14 d				
Rim		Hemosiderin	Intracellular	Hypointense	Hypointense
Center		Hemichromes	Extracellular	Isointense	Hyperintense

Adapted from W G Bradley J. MR appearance of hemorrhage in the brain. Radiology 1993;189(1):15-26; with permission.

[§]Compared to the signal intensity of normal brain parenchyma.